Wave Reflection Effects Within a Harbour

By

Enda Joseph O'Sullivan

B.E., National University of Ireland, 1990

A THESIS SUBMITTED IN PARTIAL FULFILMENT OF

THE REQUIREMENT FOR THE DEGREE OF

Master of Applied Science

in

The Faculty of Graduate Studies

Department of Civil Engineering

We accept this thesis as conforming

to the required standard

———

The University of British Columbia

March 1992

In presenting this thesis in partial fulfilment of the requirements for an advanced degree at the University of British Columbia, I agree that the Library shall make it freely available for reference and study. I further agree that permission for extensive copying of this thesis for scholarly purposes may be granted by the head of the department or by his or her representatives. It is understood that copying or publication of this thesis for financial gain shall not be allowed without my written permission.

Department of Civil Engineering,
The University of British Columbia,
2324 Main Mall,
Vancouver, B.C.,
Canada, V6T 1Z4.

Date : _24th March 1992_

Abstract

This thesis summarizes a numerical model used to predict the wave field in a harbour of constant depth with partially reflecting boundaries, and describes laboratory tests undertaken to assess the numerical model and the importance of partial reflection effects. The numerical model is based on linear diffraction theory, and involves the application of a partial reflection boundary condition. The extension to general harbour configurations that includes breakwaters is made by utilizing a wave doublet representation of the fluid boundaries instead of the usual wave source representation. The numerical model is initially compared to closed-form results for the fundamental case of a straight impermeable offshore breakwater, and the method is found to compare well for this case. Further comparisons are made for a semi-circular harbour with a pair of symmetrical protruding breakwaters, and for a rectangular harbour with a pair of symmetrical protruding breakwaters. The boundaries of the semi-circular harbour were perfectly absorbing and the numerical model predicts the wave field within the harbour realistically. For the later configuration cases which are considered include perfectly absorbing, perfectly reflecting and partially reflecting harbour boundaries, and in all cases the numerical model predicts the wave field within the harbour realistically.

Experiments were conducted at the Ocean Engineering Centre at BC Research, Vancouver. During the experiments the wave field within a model harbour was measured under different conditions corresponding to changes in the wave period, incident wave direction, incident wave height, and reflection coefficients of the harbour boundaries and breakwaters. The experimental results are compared to those of the numerical model and agreement is generally good. In general the wave heights within the harbour are slightly underpredicted, while the wave heights outside the harbour are slightly overpredicted. Overall, the numerical model is found to provide a reasonably reliable means of predicting the wave field within a harbour of constant depth and arbitrary shape with partially reflecting boundaries.

Table of Contents

List of Tables

List of Figures

List of Photographs

List of Symbols

The following symbols are used in this thesis:

$$A = -\frac{igH}{\omega},$$

C = wave celerity,

d = water depth ,

g = gravitational constant,

$G(x,\xi)$ = Green's function for a wave doublet,

H = wave height,

H_i = incident wave height,

$H_m^{(1)}$ = Hankel function of the first kind and order m,

$i = \sqrt{-1}$,

k = wave number,

L = wavelength,

n = surface normal vector at segment centre (see Figure 2.1),

n = distance in the direction of normal,

N = number of segments,

r = distance between x and ξ,

S = fluid boundary,

S_1 = one-sided boundary,

S_2 = two-sided boundary,

t = time,

T = wave period,

x = position vector given by (x, y) in the two dimensional problem (see Figure 1.1),

z = vertical coordinate measured upwards from the still water level,

α = angle between r and surface normal n (see Figure 2.1),

β = angle between r and the doublet axis (see Figure 2.1),

ΔS = segment length,

Φ = velocity potential,

ϕ = velocity potential function,

ϕ_w, ϕ_s = incident and scattered wave components of ϕ,

η = free surface elevation,

θ = wave direction measured anti-clockwise relative to the x axis (see Figure 1.1),

ω = wave angular frequency,

ξ = position vector given by (ξ,η) giving the location of Green's function on the fluid boundary (see Figure 2.1).

Acknowledgment

The author would like to thank his supervisor Dr. Michael Isaacson for his guidance and encouragement throughout the preparation of this thesis.

The author would like to express a special word of gratitude to Mr. John Baldwin for his help in explaining and running the numerical model and to Mr. Sundar Prasad for his help with the computing facilities at UBC. Thanks also to the staff of the Ocean Engineering Centre at B.C. Research, Vancouver, in particular Mr. M. Shaver, for their help throughout the experimental sequence carried out at their facilities. A special acknowledgment is made to Naomi, Reddy, Dave, Mike, Andrew, and Amal for volunteering their time, to help in the construction of the experimental layout. Without their help, the experimental sequence would surely have taken twice as long.

Finally, the financial support of a Research Assistantship from the Natural Sciences and Engineering Research Council of Canada is gratefully acknowledged.

Chapter 1
Introduction

1.1 General

A primary consideration in the design of harbours is the degree of protection afforded to vessels within the harbour. Consequently the prediction of the wave field within a harbour is of major concern to the design team planning the harbour. In developing such predictions, it should be borne in mind that the wave field within the harbour may be influenced by a combination of wave transformation effects, including wave shoaling, wave diffraction, wave refraction, wave reflection, wave breaking and wave run-up.

Over the years both experimental and theoretical approaches to the solution of wave transformations in a harbour have been developed. The most fundamental theoretical approach has dealt primarily with the problem of wave diffraction around breakwaters in a harbour of constant depth. However, these calculations have either ignored wave reflection off interior boundaries of the harbour, or else have treated all boundaries as fully reflecting. Since partial reflections are not accounted for, these approaches may give rise to incorrect predictions of the wave field. Closed-form solutions for wave diffraction around a straight semi-infinite breakwater, and a gap between a pair of co-linear straight, semi-infinite breakwaters are often used in marina design for estimating short wave diffraction into marinas. In order to treat the more general case of harbours and/or breakwaters of arbitrary configuration, as indicated in Fig. 1.1, research into the development of suitable numerical approaches has been underway for some time. Bearing in mind the ultimate objective of treating the general case of a harbour of arbitrary shape, with breakwaters and with partial reflection, Isaacson and Baldwin (1991) recently presented a numerical method of predicting the wave field in a harbour using a wave doublet distribution along the fluid boundaries. The wave doublet distribution is not as widely used as the conventional wave source distribution.

The method is based on linear diffraction theory and gives rise to an integral equation based on a wave doublet distribution along the fluid boundaries. Advantages of a doublet distribution over a source distribution are:

(i) breakwaters can be modelled. Unlike a doublet distribution, a source distribution cannot model a thin breakwater because the boundary conditions on both sides cannot be modelled simultaneously when the breakwater is treated as very thin.

(ii) partial reflection along the boundaries can be modelled. For one-sided boundaries along a harbour contour the doublet distribution can be extended to include the case of partial reflection. In the case of a two-sided boundary, corresponding to a thin breakwater, the scattered potential may be represented as due to a distribution of both wave sources and wave doublets.

The use of a doublet or dipole distribution is well known from classical hydrodynamics (Lamb, 1932) but little has been reported on its use to solve problems of water wave diffraction (Mei, 1978, Yeung, 1982, Hess, 1990).

Isaacson and Baldwin (1991) compared their formulation to the fundamental case of a straight impermeable offshore breakwater for which a closed-form solution is available and the method compared well. Further comparisons were made with more general diffraction problems such as a circular cylinder, rectangular harbour, and a circular harbour with protruding breakwaters, and in all cases excellent agreement with known solutions was obtained.

The lack of previous work based on the wave doublet representation of the fluid boundaries prompted the present research to try to verify or calibrate the numerical model using experimental results. A harbour of arbitrary shape with both two-sided fully-reflecting boundaries, and one-sided partially-reflecting boundaries is modelled by using wave doublet representations of the fluid boundaries.

1.2 Literature Review

A number of theoretical analyses have been carried out to investigate wave diffraction phenomena neglecting the effects of interior boundary reflection. Penny and Price (1952) published a solution of the boundary value problem for small amplitude waves impinging on a single semi-infinite straight breakwater, based on the equivalent problem in optical diffraction which had earlier been solved rigourously by Sommerfeld. This was verified by experimental data presented by Putman and Arthur (1948). Wiegel (1962) used Penny and Price's theoretical approach to study wave diffraction around a single breakwater and presented tables of diffraction coefficients and corresponding diffraction diagrams. These are also given in the 'Shore Protection Manual' (1984), and in other texts.

The theory of diffraction of water waves which are incident normally through a gap between a pair of coliner, straight semi-infinite breakwaters was also described by Penny and Price (1952). Their theoretical work was in agreement with the experimental work carried out earlier by Blue and Johnson (1949). Johnson (1951) developed an approximate analytical solution to obtain diffraction patterns for waves approaching a gap between a pair of semi-infinite colinear breakwaters from various wave directions. More recently, this solution was extended to non-colinear breakwaters by Memos (1980). Sobey and Johnson (1986) investigated narrow breakwater gaps, typical of smaller gaps where available results were sparse, and extended the technique to angled incidence for wide breakwater gaps and generally to non-aligned breakwaters.

Kos and Kilner (1987) carried out a set of experiments dealing with pure wave diffraction through a breakwater gap. They eliminated the effects of reflected waves, cross waves and basin resonance effects.

The above cases all relate to short wave diffraction into a harbour so that wave reflections off the harbour boundaries are neglected. On the other hand, long wave resonance in a harbour is

governed by complete reflection along the boundary. For this case Hwang and Tuck (1970) presented a numerical procedure by representing the harbour boundary as a distribution of wave sources with strengths chosen to ensure that the full reflection boundary condition is satisfied along the boundary. An alternative approach proposed by Lee (1971) involves dividing the fluid into two regions, one within the harbour and the other exterior to the harbour, and applying matching conditions at the boundary between the regions. Mattioli and Tinti (1980) extended this method to harbours with a projecting breakwater or headland. In a variant of the method, Chen and Mei (1974) used a finite element solution for the interior region matched to a boundary integral solution for the exterior region. The special cases of resonance in a rectangular harbour has been investigated by Miles and Munk (1961), Garrett (1970) and Mei (1983).

The problem of partially reflecting boundaries was treated by Berkhoff (1976). The boundaries are schematized as vertical and a mixed boundary condition is used instead of the full reflection condition. Chen (1986) introduced partial reflection and bottom friction refinements to a hybrid element model of wave behaviour in a harbour. Isaacson and Qu (1990) presented a general solution for wave behaviour in a harbour of arbitrary shape and constant depth, based on the approach indicated by Berkhoff (1976) with a matching boundary and taking partial reflections into account. Isaacson and Baldwin (1991) used a wave doublet representation of the harbour boundaries, for harbours of arbitrary shape and constant depth, taking partial reflections into account.

1.3 Research Objectives

The objectives of the present investigation are:

(i)   to carry out laboratory tests with a model harbour using different interior reflection coefficients in order to investigate the wave field within the harbour, described by contours of wave height and variations of water surface elevation (η) and wave height (H) along traverses of the harbour interior.

(ii)   to streamline the numerical model of Isaacson and Baldwin (1991) and to compare its

predictions to corresponding results of the physical model.

Chapter 2
Numerical Model

2.1 Mathematical Treatment

2.1.1 Governing Equations

The general case of a harbour of arbitrary configuration and with one or more breakwaters is shown in Fig. 1.1. It is assumed that all topographical irregularities lie within the contour C where the depth is constant and that the coastline is otherwise straight and coincides with the y-axis. A train of regular small amplitude waves approaches the harbour as shown and the wave field in the vicinity of the harbour is to be determined. A coordinate system (x,y,z) is defined with x and y horizontal and z measured vertically above the still water level. The fluid is assumed incompressible and invisid and the flow is irrotational, so that the flow may be described by a velocity potential Φ which satisfies the Laplace equation within the fluid region. Provided that all barriers are considered vertical and to extend from the seabed (or deep water) up to the free surface, the velocity potential is represented as:

$$\Phi(x,y,z) = A \; \phi(x) \; \frac{\cosh[k(z+d)]}{\cosh(kd)} \; \exp(-i\omega t) \qquad [2.1]$$

where t is time, d is the still water depth, $\phi(x)$ is a two-dimensional potential function which is to be determined, and x represents a general point (x,y) in the horizontal plane. Also $A = -igH/2\omega$, $i = \sqrt{-1}$, H is the incident wave height, k is the wave number, and ω is the angular frequency which is related to the wave number by the linear dispersion relation:

$$\omega^2 = gk \tanh(kd) \qquad [2.2]$$

Eq. [2.1] directly satisfies the seabed and free-surface boundary conditions. In addition, the potential function ϕ itself must satisfy the Helmholtz equation within the fluid region and is also

subject to a boundary condition along the fluid boundaries and to a radiation condition. In the case of complete reflection at impermeable boundaries, the boundary condition corresponds to that of zero normal velocity along the fluid boundary:

$$\frac{\partial \phi}{\partial n} = 0 \qquad\qquad [2.3]$$

where n is the distance normal to the fluid boundary as indicated in Fig. 1.1.

It is convenient to express the potential function ϕ as a superposition of a known incident wave potential ϕ_w and a scattered wave potential ϕ_s:

$$\phi = \phi_w + \phi_s \qquad\qquad [2.4]$$

The incident wave potential ϕ_w is known and may be expressed as:

$$\phi_w (x) = \exp [\ ik\ (x\cos\theta + y\sin\theta)] \qquad\qquad [2.5]$$

where θ is the incident wave direction measured from the x axis as shown in Fig. 1.1.

Solving for ϕ_s is the crux of the problem, since a solution for ϕ_s then directly provides ϕ. Any required property of the wave field may then be obtained. In summary, ϕ_s satisfies (i) the Helmholtz equation, (ii) the radiation condition, and (iii) the reflection boundary condition.

2.1.2   Extension to Partial Reflection

For the more general case of wave diffraction in harbours, neither the assumption of fully absorbing or fully reflecting boundaries is really appropriate since in practice partial reflection invariably occurs within a harbour. A boundary condition corresponding to partial reflection may be introduced in the manner used by Chen (1986), and Isaacson and Qu (1990). This takes the form of a mixed boundary condition :

$$\frac{\partial \phi}{\partial n} + \alpha\ k\ \phi\ = 0 \qquad\qquad [2.6]$$

in which n is distance into the fluid region measured normal to the boundary and α ($= \alpha_1 + i\alpha_2$) is a complex transmission coefficient. This coefficient may be interpreted in a number of different ways as summarized by Isaacson and Qu (1989). These relate to;

(i)   its relation to the rate of transfer of energy at the boundary,

(ii)   its relation to the height and phase of the wave field at the boundary,

(iii) its relation to the conventional reflection coefficient.

In particular, the transmission coefficient α ($= \alpha_1 + i\alpha_2$) may be related to the reflection coefficient K_r and a phase shift β associated with the reflection, and the angle γ which the incident wave train makes with the normal to the boundary. Assuming the wave train undergoes oblique reflection from a vertical wall located at x = 0, the total potential of the combined wave field corresponds to a three-dimensional wave pattern and may be written as the sum the incident and reflected wave potentials;

$$\phi = A\{\exp[ik \ (x \cos \gamma + y \sin \gamma)] + K_r \exp[-ik \ (x \cos \gamma - y \sin \gamma) + i\beta]\} \quad [2.7]$$

Here K_r is defined as the ratio of the reflected wave height to the incident wave height. Substituting Eq. [2.7] into Eq. [2.6], the transmission coefficient α is given as:

$$\left. \begin{array}{l} \alpha_1 = \dfrac{2K_r \sin \beta \ \cos \gamma}{1 + K_r^2 + 2 \ Kr \cos \beta} \\[4mm] \alpha_2 = \dfrac{(1 - K_r^2) \cos \gamma}{1 + K_r^2 + 2K_r \cos \beta} \end{array} \right\} \qquad [2.8]$$

For the particular case of normally incident waves ($\gamma = 0°$) and $\beta = 0°$ may be expressed in terms of the conventional reflection coefficient K_r as:

$$\left. \begin{array}{l} \alpha_1 = 0 \\[3mm] \alpha_2 = \dfrac{1 - K_r}{1 + K_r} \end{array} \right\} \qquad [2.9]$$

2.1.3 Green's Function Representation

The boundary value problem which has been specified is solved by expressing the scattered potential at any point x in the fluid domain as due to a distribution of wave doublets on the fluid boundary S:

$$\phi_s(x) = \frac{1}{4\pi} \int_S \mu(\xi)\, G(x;\xi)\, dS \qquad [2.10]$$

where $\mu(\xi)$ represents the doublet strength distribution function, $\xi = (\xi,\eta)$ is the doublet location along the fluid boundary S and G is a known Green's function for a wave doublet. This corresponds to a fundamental solution of the Helmholtz equation which satisfies the radiation condition, and is given as:

$$G(x;\xi) = i\,\pi\, H_1^{(1)}(kr)\, \cos\beta \qquad [2.11]$$

where $r = |x - \xi| = \sqrt{(x-\xi)^2 + (y-\eta)^2}$, β is the angle at the doublet location which the point x makes with the doublet axis taken normal to the surface contour as shown in Fig. 2.1 and $H_1^{(1)}$ is the Hankel function of the first kind and order one.

The application of the boundary condition Eq. [2.3] for the general case of partial reflection gives rise to the following integral equation for $\mu(\xi)$:

$$\frac{1}{4\pi} \int_S \mu(\xi)\, \frac{\partial G(x;\xi)}{\partial n}\, dS + \frac{k\,\alpha(x)}{4\pi} \int_S \mu(\xi)\, G(x;\xi)\, dS = -\frac{\partial \phi_w}{\partial n}(x) - k\,\alpha(x)\,\phi_w(x) \quad [2.12]$$

where x is the point on S at which the boundary condition is applied, and n is the normal vector to S at x. In the case of a fully reflecting portion of the boundary, $\alpha = 0$ so that the second integral in Eq. [2.12] is then absent. In the case of a fully absorbing portion of the boundary, $\alpha = i$ and the radiation condition is satisfied directly so that this portion of the boundary can then simply be omitted from Eq. [2.12]. Along one-sided boundaries S_1, the Green's function may be taken as

either a wave source or wave doublet, although it is customary to use the wave source (eg. Hwang and Tuck, 1970). In Eq. [2.12] the Green's function has been taken to be a wave doublet and it will be shown here that this provides a practical alternative to wave source methods. Along two-sided boundaries S_2, the wave source representation is no longer appropriate since a source distribution involves a velocity discontinuity across the contour of the distribution. A wave doublet avoids this difficulty and may be used to simultaneously satisfy the boundary condition of full reflection on both sides of a breakwater, Hunt (1980). The extension to partial reflection implies that the velocity potential must be represented as due to a distribution of both wave sources and wave doublets. This refinement gives rise to numerical difficulties and has not yet been developed so that in the present study two-sided boundaries are taken to be fully reflecting. Thus α is then zero and the second integral in Eq. [2.12] is omitted for x on S_2.

In evaluating the integrals in Eq. [2.12], the derivative of the Green's function $\partial G/\partial n$ is required. This may be expressed as:

$$\frac{\partial G}{\partial n}(x;\xi) = -i\pi \left\{ \frac{H_1^{(1)}(kr)}{r} \cos(\gamma+\beta) - k\, H_0^{(1)}(kr) \cos\gamma \cos\beta \right\} \qquad [2.13]$$

where $H_0^{(1)}$ is the Hankel function of first kind and order zero, and γ and β are indicated in Fig. 2.1 and are related to the normal vectors at x and ξ:

$$\cos\gamma = \frac{n_x^x(x-\xi) + n_y^x(y-\eta)}{r} \qquad [2.14]$$

$$\cos\beta = \frac{n_x^\xi(x-\xi) + n_y^\xi(y-\eta)}{r} \qquad [2.15]$$

where n_x and n_y are the direction cosines of the normal vector n with respect to the x and y directions, and the superscript denotes the location at which the direction cosines are evaluated.

2.2 Numerical Approximation

The integral equation is solved by a discretization process in which the fluid boundary is divided into N short straight segments, and the doublet strength distribution is assumed constant over each segment. In this way the integral equation is transformed into a matrix equation:

$$\sum_{j=1}^{N} B_{ij}\, \mu_j = b_i \qquad\qquad [2.16]$$

where

$$b_i = -\frac{\partial \phi_w}{\partial n}(x_i) - k\, \alpha(x_i)\, \phi_w(x_i) \qquad\qquad [2.17]$$

$$B_{ij} = \frac{1}{4\pi} \int_{\Delta S_j} \frac{\partial G}{\partial n}(x_i;\xi_j)\, dS + k\, \alpha(x_i)\, \frac{1}{4\pi} \int_{\Delta S_j} G(x_i;\xi_j)\, dS \qquad\qquad [2.18]$$

and ΔS_j is the length of the j-th segment, x_i denotes the centre of the i-th segment, and the integrations apply to the moving point ξ.

The evaluation of the matrix coefficients B_{ij} is carried out separately for the first and second integrals in Eq. [2.18]. For $i \neq j$, the second integral is evaluated by the usual mid-point approximation. However, for the first integral the normal velocity induced by one segment on a neighbouring segment is not small, so that a mid-point approximation is unsuitable and a numerical integration is then necessary. This has been carried out using a 4 point Gaussian quadrature rule (e.g. Brebbia and Walker, 1980), with care taken to include the variation of γ and β along the segment length. When $i = j$, a singularity occurs in both integrals so that an analytic integration is then used. Retaining the leading terms in expansions for $\partial G/\partial n$ and G near the singularity a suitable approximation for B_{ii} is given as:

$$B_{ii} = -\frac{2}{\pi k \Delta S} - \frac{k\Delta S}{4\pi}\left\{\ln\left(\frac{k\Delta S}{4\pi}\right) - 1\right\} + i\,\frac{k\Delta S}{8} + \frac{\alpha}{2} \qquad\qquad [2.19]$$

where the higher order terms, though not strictly required for convergence, have been found to greatly increase the performance of the method.

Once the matrix coefficients B_{ij} have been evaluated, Eq. [2.16] can be solved by a standard complex matrix inversion procedure to provide the doublet strengths μ_j. The potential function, ϕ_s at a general point x, may then be obtained from a discretized version of Eq. [2.10]:

$$\phi_s(x) = \frac{1}{4\pi} \sum_{j=1}^{N} \mu_j \, G(x;\xi_j) \, \Delta S_j \qquad [2.20]$$

where, as a consistent approximation, G is assumed constant over the segment length and a mid-point approximation is used. If the point x lies on the boundary, a singularity occurs when x is at j and an integration of the leading singular term gives:

$$\phi_s(x_j) = \pm \frac{1}{2k} \mu_j \qquad [2.21]$$

where the positive sign corresponds with the definition of the surface normal.

Once ϕ_s and hence ϕ are known, then any required property of the wave field may be obtained. In particular, the water surface elevation η at time $t=0$ is useful in obtaining a general view of the wave field at a particular instant, and the diffraction coefficient K_d describes the variation of the wave heights within the harbour. These are given as:

$$\eta = \frac{1}{2} \text{Re} \, (\phi) \qquad [2.22]$$

$$K_d = |\phi_w + \phi_s| \qquad [2.23]$$

Chapter 3
Physical Model

3.1 Experimental Facilities

A set of laboratory experiments relating to the wave field within a harbour were conducted at the Ocean Engineering Centre (OEC) at BC Research, Vancouver during November 1991. The Centre is operated by the British Columbia Research Corporation, under an agreement between BC Research, the University of British Columbia, and the National Research Council of Canada (NRC).

The wave basin at OEC measures 30.5 m x 26.5 m (100 ft x 87 ft) with a maximum operating depth of 2.4 m (8 ft) deep (see Fig. 3.1). The basin is equipped with a unidirectional wavemaker, and a modern VAX computer system. The dimensions of the wavemaker are 15 m x 1.8 m (50 ft x 6 ft). It may be relocated within the basin in order to provide for the propagation of waves from a number of different directions. The wavemaker may be operated in a number of different modes which can be selected by adjusting a mechanical pivot point. The wavemaker may be operated in either a piston mode, a hinged flapper mode, or a combined mode with equal contributions of piston/flapper. This allows for the accurate simulation of shallow, intermediate and deep water waves.

Wave absorber modules may be positioned around the basin so as to minimise the corruption of the measured wave field by wave reflections from the basin walls . These wave absorbers are made from two sheets of 0.6 m x 3 m perforated metal fixed 0.3 m apart by timber blocks. The absorbers are portable and work by dispersing the wave energy as it passes through the perforated metal.

The wave generation, data acquisition and analysis is carried out using the GEDAP software system. GEDAP was developed at the NRC Hydraulics Laboratory in Ottowa and is an acronym for Generalized Experiment control, Data acquisition and data Analysis Package.

3.2 Model Harbour

The hypothetical model was conceived on the basis of a harbour at Comox, B.C., Canada (see Fig. 3.2). Fig. 3.3 shows the harbour at Comox in detail, including depth soundings and breakwater lengths. It should be noted that the marina located to the left of the breakwater has since been relocated to the right of the breakwater (i.e. inside the new harbour).

In planning the model harbour layout, a length scale ratio of 1:50 was found to be suitable, and the water depth was kept constant at 450 mm. On the basis of Froude scaling, the time scale ratio is $1:\sqrt{50}$. A view of the physical model is shown in Photograph 3.1 and a sketch of the model is given in Fig. 3.4.

The model experiments can be divided into three different phases as indicated in Fig. 3.5. In Phase 1, both the breakwater and the harbour interior represented fully reflecting vertical walls. This was accomplished by constructing the harbour boundaries from vertical sheets of plywood (see Fig. 3.6 (a), (c)), with hardboard used for the curved portions of the boundaries as shown in Photograph 3.4. In Phase 2, the breakwater remained fully reflecting while the interior harbour boundaries were changed to represent a partially reflecting beach. In order to achieve this, the plywood and hardboard were replaced by a beach of slope 1:2.5, which was comprised of sand overlain by a layer of artificial horsehair as shown in Fig. 3.6 (d) and Photograph 3.5. In Phase 3, the breakwater was changed to represent a partially reflecting rubblemound breakwater (see Fig. 3.6 (b)) and the harbour interior remained a partially reflecting beach (see Photograph 3.6). The rubblemound breakwater was represented by placing rocks, of mean diameter 60 mm, against the existing plywood breakwater at a slope of 1:1.5. While running the tests for Phase 1 a considerable interval was required to allow for dissipation of the wave energy.

The wavemaker at BC Research has four sections on the wave board. In order to minimise the amount of wave energy produced, the two end sections of the wave board were disconnected. As a result the wavemaker had to be calibrated. To do this calibration a 2-dimensional wave flume, 3 m wide, was placed orthogonal to the wave board face. This enabled the measurement of the wave produced by the wavemaker without interference from wave reflections, diffraction and other distortions.

3.3   Dimensional Analysis

In planing the model tests and presentation of results, it is useful to carry out a dimensional analysis of the problem in order to identify the governing parameters so that controlled variables in the model could be suitably varied. For regular incident waves and a specified harbour configuration, the wave height H at any location within the harbour may be expressed in the form:

$$H = f \ (H_i, \ \theta, \ d, \ L, \ g, \ x, \ y) \hspace{3cm} [3.1]$$

where

H_i is the incident wave height,

θ is the angle of wave incidence,

d   is the still water depth,

L   is the wavelength,

g   is the acceleration due to gravity,

(x,y) is the position inside the harbour.

Note that the wave celerity c or wave period T are not specifically identified since these may be expressed in terms of d, g and L by linear wave theory.

The application of dimensional analysis to Eq. [3.1]then provides:

$$\frac{H}{H_i} = f \left\{ \frac{x}{L}, \frac{y}{L}, \frac{d}{L}, \frac{H_i}{L}, \theta \right\} \hspace{3cm} [3.2]$$

The wave steepness H_i/L may be omitted if nonlinear effects are ignored. In Eq. [3.1] H/H_i corresponds to the diffraction coefficient K_d. Consequently, the diffraction coefficient may expressed in the form:

$$K_d = \frac{H}{H_i} = f\left\{\frac{x}{L}, \frac{y}{L}, \frac{d}{L}, \theta\right\}$$ [3.3]

Thus, in carrying out tests for a specified harbour configuration subjected to regular waves, contour plots of the diffraction cofficient may be obtained for different incident wave directions θ, and different values of d/L corresponding to changes in the wave period. In addition, since the primary focus of the present study is an examination of the effects of the reflectivity of the harbour boundaries, contour plots would also be required for different degrees of reflectivity.

3.4 Wave Elevation Measurement

Capacitance wave probes were used to measure the instantaneous water surface elevation. Water level measurements made with these probes are accurate to within $\pm$ 1.0 mm, and are not influenced by spray above the continuous air/water interface.

The wave probes were calibrated by using the GEDAP calibration called RTC_NPCAL. The calibration is based on a fourth order polynomial relating the wave elevation to the corresponding sensor signal measured in volts. The corresponding fine calibration constants were computed and stored in the GEDAP port file. They were subsequently used in processing the data (see section 3.6).

It was essential to place wave elevation probes at a sufficiently large number of grid positions in order to measure the wave field throughout the interior of the model harbour. The grid spacing was small enough to provide an acceptable resolution of wave elevation information, while not resulting in too cumbersome an amount of data. The grid spacing was also prescribed by the shortest wavelength to be tested. A 0.6 m spacing was deemed appropriate.

The wave probe apparatus is shown in Fig. 3.7. It consists of an array of 14 wave probes set as two rows of 7 probes supported on a rigid frame which could be moved to the required locations with relative ease. One reference probe was located outside the harbour as indicated in Fig. 3.8. The measurement of the wave field within the harbour was achieved by moving the rectangular array of fourteen probes to three and four positions for Phases 1 & 2 and Phase 3 respectively. The corresponding areas covered in the three phases the area shown in Fig. 3.7.

3.5 Reflection Analysis

In order to ensure accurate prediction of the wave field using the numerical model, it is essential to be able to specify values of the reflection coefficients of the fluid boundaries. To this end a series of reflection analyses were carried out on the physical model.

The experimental layout for these tests is shown in Fig. 3.9. A set of two plywood guide walls, 1 m apart, were positioned perpendicular to the inner harbour boundary so as to create a two-dimensional wave field without any influence from reflection or other wave distortions, thus ensuring accurate measurement of the reflection coefficients. Three colinear wave probes were set up, with the nearest located 3 m from the boundary. A series of three tests were carried out corresponding to the three categories of boundary located at the end of the guide walls:

(i)   sand at 1:2.5 overlain with horsehair, (see Photograph 3.7),

(ii)   a vertical plywood sheet, (see Photograph 3.8),

(iii)   rocks at 1:1.5 positioned against the plywood, (see Photograph 3.9).

For each boundary, wave reflection tests were carried out for the five wave conditions used in the experiments.

The data was analysed using the program REFLM. This program separates the incident and the reflected wave from a measured wave field on the basis of a least squares analysis using data from 3 probes. The accuracy of the method decreases when the spacings between the two pairs of adjacent probes is equal (Isaacson, 1991), and consequently probe two was placed slightly off

centre such that $L_{12} = 0.95 \, L_{23}$, where L_{12} and L_{23} are the distances between the two pairs of adjacent probes. Isaacson (1991) found that this relative spacing should have good accuracy.

3.6 Wave Generation, Data Acquisition and Analysis

The GEDAP software package includes a program category denoted WAVE_GEN which contains a comprehensive set of programs for two-dimensional wave generation in laboratory flumes, towing basins and wave basins. A program RWREP2 computes the wave machine control signal for a regular wave train corresponding to a wave height and period specified by the user. The wave heights and periods may be specified in either full scale units or model scale units, since RWREP2 automatically converts these to model scale units when calculating the control signal for the wave machine. The duration of the control signal is always set to an integer number of wave periods, so that the signal can be continuously recycled when driving the wave machine. The control signal file produced by program RWREP2 is sent to the wave machine controller through a D/A output channel by using the real-time control program RTC.

The software package RTC (Real Time Control) Single User System was used in all stages of the experimental procedure. RTC consists of a main hardware execution program and a command entry program that allows the user complete control over data acquisition, control loops and signal generation.

Wave generation was carried out by first loading the control signal file into an RTC buffer file and then enabling the buffer to start the wave machine. When the enable command was given, the output signal was smoothly ramped up from zero amplitude to full amplitude over a period of 10 sec. This automatic ramping was a carried out in order to protect the wave machine from being subjected to sudden transients in its control signal.

The program RTC was also used to measure the wave train produced by the wave machine. The wave probes were sampled at a rate of 20 samples per second for a duration of 45 seconds.

The resulting data file had was demultiplexed by running the program PDMULT2 before the measured wave train could be analysed.

This program is used to demultiplex a GEDAP Primary Data File produce by the GEDAP Data Acquisition System. The demultiplexing produces individual GEDAP compatible data files that may then be analysed or plotted by existing GEDAP programs. The output data is converted to calibration units using calibration factors stored in the GEDAP Port File. The demultiplexing is base upon the polynomial function:

$$z = A + Bx + Cx^2 + Dx^3 + Ex^4 \qquad [3.4]$$

From PDMULT2 there is one output file for each wave probe. The signal from each probe can be inspected visually using GPLOT. From the plot of wave height vs time one can inspect the wave train and choose the segment or subrecord to be analysed.

SELECT1 is used to select a sub-record from a longer time series input record. The sub-record is defined by specifying T1 and T2, where T1 is the initial time of the sub-record and T2 is the final time. The selected sub-record will match T1 and T2 as closely as possible subject to the resolution limit imposed by the time step of the input record. The selected sub-record is stored in a GEDAP output file.

The sub-record can now be analysed using ZCA (Zero-Crossing Analysis of a Wave Elevation Time Series Record). ZCA performs a time-domain zero-crossing analysis on a time series signal. It is designed primarily for wave elevation records but it may also be used to analyse other types of data such as force records. ZCA performs both zero up-crossing and zero down-crossing analyses.

The program ZCA checks the time spacing of the input signal to ensure that the sampling rate is high enough for accurate zero-crossing analysis. If the input signal contains fewer than 50 points per average zero-crossing period, then it is automatically resampled using cubic spline interpolation

so that the time spacing is small enough to meet this criterion. In addition to resampling, ZCA also uses local parabolic curve fitting to define the peaks and troughs in the signal. The zero up-crossing and down-crossing times are calculated by linear interpolation so they are not limited by the sampling rate of the input signal. The parameter of interest is average wave height which is taken as the average of the average zero up-crossing wave height and average zero up-crossing wave height.

The average wave height from each of the 15 wave records are now collected using the program COLLECT, which collects individual header parameter values from several different GEDAP input files and stores them in a single data vector in a GEDAP output file. The number of input files is equal to the number of program cycles. One output file is generated for each parameter name selected.

The wave heights are then exported to the UBC main-frame computer in order to generate contour plots. This is achieved using the program EXPORT which converts one or more binary GEDAP data files to a single ASCII file with a simple format. This program is normally used to convert GEDAP data for processing by non-GEDAP programs or for transfer to non-VAX computers such as Apple Macintosh or main frame terminals. Each GEDAP input file is stored in a single column of the ASCII output file.

The contours plots are generated using the program DISSPLA on the UBC main-frame computer. Once generated, the plots are transferred to an Apple Macintosh IIx computer for printing.

3.7 Test Program

In view of the foregoing, the purpose of the experiments was to measure the wave field within the harbour under different conditions corresponding to changes in the wave period (and consequently the length), incident wave direction, incident wave height, the reflection coefficients

of the harbour boundaries and finally the reflection coefficients of the breakwaters. Table 3.1 lists the characteristics of the wave conditions tested.

The conditions were selected with respect to a base case corresponding to the following parameters:

$$\theta = 0°, \ T = 0.803 \ sec, \ H = 30 \ mm.$$

Thus Table 3.1 corresponds to the following set of tests:

(i)   the effects of wave period were examined by changing the wave period to include $T = 0.803, 0.937, 1.068, 1.20$ sec, while keeping harbour boundaries and breakwaters fully reflecting and the other parameters constant (tests 2 - 5).

(ii)   the effects of wave direction were investigated by changing the wave direction to include $\theta = +30°, 0°, -30°$, (tests 1, 2, 7).

(iii) the effects of wave height were examined by changing the wave height to include $H = 30$ mm, 15 mm (tests 1, 6).

(iv)   the series of 7 tests were repeated with the low reflecting harbour boundary and fully reflecting breakwaters (tests 8-14).

(v)   finally 6 of these tests were repeated (wave direction $\theta = -30°$ was omitted), with the low reflecting harbour boundary and the partially reflecting breakwaters (tests 15-20).

As can be seen from Table 3.1, all of the test conditions correspond to intermediate depth waves (i.e. $0.05 < d/L < 0.5$), and are in fact close to the deep water wave region (i.e. $d/L \geq 0.5$). Therefore the wave generator was used in the flapper mode, which simulates deep water wave conditions, in order to produce the required wave conditions as closely as possible.

Chapter 4
Results & Discussion

4.1 Comparison of Numerical Results with Exact Solutions

The wave doublet representation of the fluid boundaries was examined to verify its suitability. Preliminary results are presented here for cases corresponding to:

(i)   a straight offshore breakwater for which an exact solution is available,

(ii)   a breakwater gap represented by a semi-circular harbour with straight fully reflecting breakwaters and totally absorbing interior harbour boundaries. The results may be compared to the exact solution for a breakwater gap between a pair of straight, fully reflecting, colinear, semi-infinite breakwaters (Sobey and Johnson, 1986).

4.1.1   Straight Offshore Breakwater

In order to investigate the convergence of the wave doublet representation, a comparison was made to results for the wave force on a rigid vertical plate, since this force corresponds to a suitable averaged value of the velocity potential difference across the breakwater. The force F is given as:

$$F = \frac{\rho gHd}{2} \ \frac{\tanh(kd)}{kd} \int (\phi_w + \phi_s) \, n_x \, dS \, e^{-i\omega t} \qquad [4.1]$$

Table 4.1 indicates the number of segments necessary to reproduce the closed-form solution adequately and the corresponding degree of accuracy, for the particular case of the plate subjected to a uni-directional incident wave train of unit height, and propagating orthogonal to the plate ($\theta = 0°$) as indicated in Fig. 4.1. A plate length to wave length ratio of B/L = 2.0, and a still water depth to wave length ratio of d/L = 0.4 were chosen.

The ratio of the maximum horizontal force computed using N segments to the corresponding closed-form solution is tabulated for the various numbers of segments used. The table indicates

that as little as 10 segments per wave length is adequate to predict the force. A 4 point Gaussian integration of the matrix coefficients in Eq. [2.15] was used to obtain the results. Further improvements corresponding to either 8 or 16 point are not shown here, but were found to give only a marginal increase in accuracy and therefore were not warranted. The diagonal components of the matrix equation were approximated to the second order.

For breakwater applications it is the wave height distribution around the breakwater that is of practical interest rather than wave force. Fig. 4.2 shows a comparison of the distribution along the breakwater contour for the same conditions as before: B/L = 2.0, d/L = 0.4 and θ = 0°. The breakwater extends along the y-axis from y/L = ±1. The distributions of the wave height along the upwave (exposed) and downwave (sheltered) sides of the breakwater are shown in Fig. 4.2 (a) and 4.2 (b) respectively. Numerical solutions for N = 10 and N = 20 are compared to the closed-form solution, and the solution obtained using N = 20 is seen to show excellent agreement with the closed-form solution.

Of more general interest is the wave height distribution in the vicinity of the breakwater, and the corresponding contours of the wave height are shown in Fig. 4.3 for the same conditions as before, and with N = 50. Once more excellent agreement with the closed form solution is obtained. A three-dimensional view of the water surface elevation in the vicinity of the breakwater at the particular instant t = 0 is shown in Fig. 4.4, and serves to confirm that the general form of the wave field in the region near the breakwater is as anticipated. The figure clearly shows the wave build-up in the upwave region and a wave height reduction in the leeward (sheltered) region of the breakwater.

4.1.2 Breakwater Gap

In order to investigate the accuracy of the wave doublet representation of the harbour boundaries, numerical results for a semi-circular harbour with protruding breakwaters as shown in Fig. 4.5, with fully reflecting breakwaters and fully absorbing harbour boundaries, was compared

to the closed-form solution for the case of a gap between a pair of straight, fully reflecting, colinear, semi-infinite breakwaters. The harbour has a radius of 350 m and a gap width of 50 m between the pair of symmetrical breakwaters.

The harbour was subjected to a uni-directional incident wave train of unit wave height, propagating orthogonal to the breakwater gap ($\theta = 0°$) as indicated in Fig. 4.5. The wave period of T = 5.7 sec, depth of d = 20 m corresponds to a wave length L = 50 m which gives a breakwater gap to wave length ratio B/L = 1.0.

Fig. 4.6 shows a comparison of the contours of the diffraction coefficient in the vicinity of the breakwater gap. The wave field is symmetric so that only one half is shown. The breakwater gap extends along the y axis between y/L = $\pm$ 0.5. The solution obtained corresponds to 10 segments per wave length. The wave doublet representation is seen to show very good agreement with the exact solution.

A three-dimensional view of the surface elevation at the particular instant t = 0 in the vicinity of the breakwater gap is shown in Fig. 4.7. The general form of the wave field is as expected, exhibiting the expected features of wave crests which approximately form concentric arcs centred at the middle of the breakwater gap, and wave heights which noticeably decrease in the shadow zone behind the breakwaters and which are close to the incident wave height outside of the shadow zone. This figure serves to confirm visually that the wave doublet representation of the wave field yields satisfactory results.

4.2 Effects of Reflection Coefficients

The wave doublet representation of the fluid boundaries enables the representation of one-sided partially reflecting boundaries along with two-sided fully reflecting boundaries. In an effort to investigate the performance of this method, the numerical model was applied to the fundamental case of a rectangular harbour with protruding breakwaters as shown in Fig. 4.8. The harbour has a length of 300 m, a width of 300 m, and a gap width of 50 m between the pair of symmetrical

breakwaters. The harbour was subjected to a uni-directional incident wave train of unit wave height, propagating orthogonal to the breakwater gap ($\theta = 0°$) as indicated in Fig. 4.8. The wave period of T = 5.7 sec, depth of d = 20 m corresponds to a wave length L = 50 m which gives a breakwater gap to wave length ratio B/L = 1.0. The fully reflecting breakwaters and the partially reflecting harbour boundaries are represented by wave doublets.

The wave field within the harbour predicted by the present method for the case of fully absorbing boundaries and impermeable breakwaters is shown in Fig. 4.9 and 4.10. Fig. 4.9 shows the contours of diffraction coefficients which are compared to the predictions of the analytical solution for a pair of colinear breakwaters. As can be seen the wave field is similar to the analytical solution for example the wave heights diminish along the breakwaters. The wave doublet representation of the rectangular harbour is seen to show very good agreement with the exact solution. Fig. 4.10 shows a view of the computed free water surface elevation at time t = 0. This exhibits the expected features of wave crests which approximately form concentric arcs with centres at the middle of the breakwater gap.

In comparison to this case, Fig. 4.11 and 4.12 show corresponding results for the identical conditions, except that the boundaries of the harbour are fully reflecting, $K_r = 1.0$. This case of full reflection was considered by Miles and Munk (1961), Garrett (1970), and Mei (1983) in the context of harbour resonance. The diffraction coefficient contours within the harbour are shown in Fig. 4.11, while Fig. 4.12 shows the computed free surface elevation at time t=0, indicating a generally confused, three-dimensional wave field within the harbour.

The more general case of boundaries with partial reflection corresponding to a reflection coefficient of $K_r = 0.1$ is shown in Fig. 4.13 and 4.14. For the relatively low value of reflection coefficient adopted here, the results are not too different from the case of fully absorbing boundaries as already indicated in Fig. 4.9 and 4.10. The diffraction coefficient contours show a slight increase in the wave energy in the harbour (Fig. 4.13). However Fig. 4.14 shows no significant differences from the corresponding results for fully absorbing boundaries (Fig. 4.10).

Fig. 4.15 compares the wave height contours for the example problem being considered, but with the reflection coefficient along the harbour boundaries taken as $K_r = 0$, 0.1 and 0.2 in turn. The figure shows an increasing irregularity in the diffraction coefficient contours as a transition to the more confused state of full reflection, indicated in Fig. 4.11 is being approached.

4.3 Numerical and Experimental Analysis of Harbour

4.3.1 Experimental Results

The purpose of the experiments was to measure the wavefield within the harbour under different conditions corresponding to changes in the wave period (and consequently the length), incident wave direction, incident wave height, the boundary reflection characteristics of the harbour boundaries and finally the reflection coefficients of the breakwaters. The experimental layout shown in Fig. 3.4 was subjected to a total of 20 test runs (see Table 3.1).

4.3.1.1 Effect of Wave Period

Four wave periods were used in the experiments as indicated in Table 3.1 (T = 0.8, 0.94, 1.07, 1.2 sec). The reference probe (Fig. 3.8) did not function during one of the tests in this set (test 2, T = 0.8 sec) so that the corresponding plot is absent. Fig. 4.16 shows the diffraction coefficient contour plots for the different periods (except one), used for Phase 1 of the tests, corresponding to highly reflective harbour boundaries and breakwaters. The contours indicate a confused wave field corresponding to standing waves within the harbour. On close examination, the contour plots show some unacceptable features, including contours crossing and relatively jagged contours. These effects may be due in part to an imperfect contouring program and in part to the relatively course spacing of the wave probes used to measure the wave field. (A spacing of 0.6 L_{min} = 600 mm, was chosen). The wave lengths of the standing waves in the harbour appear to have been considerably shorter than this value. This combined to seems to have given rise to the poor quality of the contour plots. It is difficult to extract any useful results from these plots.

Fig. 4.17 shows diffraction coefficient contour plots for the four periods used for Phase 2 of the tests, corresponding to highly reflective breakwaters and partially reflecting beaches. In all cases the wave heights now decrease significantly in the shadow region as expected. The general trend of increased wave heights in the shadow region with increasing wave period is in agreement with standard results (e.g. Shore Protection Manual, 1984).

Fig. 4.18 shows the diffraction coefficient contour plots for the four periods used for Phase 3 of the tests, corresponding to partially reflecting breakwaters and partially reflecting beaches. Once more the wave heights decrease significantly in the shadow region. There is little change in the plots with increasing period except for the largest period (T = 1.2 sec) which shows a slight decrease in the wave heights near the tip of the breakwater. This may be due to inaccurate measurement, rather than indicating a general trend.

4.3.1.2 Effect of Incident Wave Direction

Three incident wave directions were used throughout the experiments: θ = -30°, 0°, +30° (see Fig. 3.4). Fig. 4.19 shows the diffraction coefficient contours for the three directions with T = 0.8 sec for the Phase 2 set of tests with increasing angle of incidence. As expected, a greater level of wave energy enters the harbour, indicated by the contours extending further into the harbour. A comparison of Figs. 4.19 (a) and 4.19 (c) indicates that the difference is quite appreciable emphasising the importance of adequately accounting for the incident wave angle.

In Fig. 4.19 (c) the contours may not be as accurate as one would like (the 0.8 contour should not change orientation). This may be due to the reference probe miss-reading the wave height. It is probable however that the general appearance of the contours is relatively accurate.

4.3.1.3 Effect of Boundary Reflection Characteristics

A total of three combinations of reflection coefficients were used throughout the experiments corresponding to the three Phases of the tests. Phase 1 corresponds to a highly reflecting

breakwater and fully reflecting harbour boundaries; Phase 2 corresponds to a highly reflecting breakwater and partially reflecting harbour boundaries; and Phase 3 corresponds to a partially reflecting breakwater and partially reflecting harbour boundaries. The three corresponding configurations are sketched in Fig. 3.5.

The diffraction coefficient contours for each of the three Phases and for T = 0.94 sec are shown in Fig. 4.20. The diffraction coefficient contours for Phases 2 and 3 show a pattern similar to that for the case of a semi-infinite breakwater (Shore Protection Manual, 1984) since the interior harbour boundaries have a relatively low degree of reflectivity. On the other hand the contours for Phase 1 show a more confused wave field associated with the presence of standing waves which were observed. The highly reflecting boundaries prevented the dissipation of wave energy at the harbour boundaries.

The difference in diffraction coefficient contours between Fig. 4.20 (a) and (c) emphasises the importance of accounting for the reflectivity of the harbour boundary.

4.3.1.4 Effect of Incident Wave Height

Two incident wave heights were used throughout the experiments. The nominal incident wave height was 30 mm for most of the tests, whereas this was reduced to 15 mm test 6, 13 and 20, corresponding to T = 0.8 sec for each of the three phases. In order to indicate the influence of wave height, Fig. 4.21 shows a comparison between the results of test 13 and 9 corresponding to the two wave heights but otherwise identical conditions (Phase 2, T = 0.8 sec, $\theta = 0°$). The figure shows the diffraction coefficient along a traverse at y = 2.1 m. In both cases the wave heights decrease significantly in the shadow region and the diffraction coefficients are very similar indicating that the diffraction coefficient is independent of wave height. As indicated earlier the reference probe did not function during test 2, therefore the comparison between test 6 and test 2 cannot be made.

Fig. 4.22 shows a corresponding comparison between the results of test 20 and 16 corresponding to the two wave heights but otherwise identical conditions (Phase 3, T = 0.8 sec, $\theta = 0°$). The diffraction coefficient along a traverse at y = 2.2 m is shown, and once more the wave heights decrease significantly in the shadow region and the diffraction coefficients are very similar indicating that the diffraction coefficient is independent of wave height.

4.3.1.5 Measured Reflection Coefficients

The reflection coefficients of the vertical plywood, sand covered by horsehair at a slope of 1:2.5, and the rocks at a slope of 1:1.5 were measured during the physical experiments. The results are summarized in Table 4.2. These results did not exhibit any trends (i.e. no apparent relationship between reflection coefficient and either wave period or wave height).

4.3.2 Comparison of Numerical and Experimental Results

The harbour configuration used for the numerical modelling is shown in Fig. 3.4. In setting up the numerical model the fluid boundaries were divided into short segments of length of 0.1 m corresponding to one tenth of the shortest wave length (1 m) as recommended in section 4.1.1. To test the harbour using the numerical model, the coordinates and reflection coefficients of each segment was specified. All the fluid boundaries (coastline, breakwaters and harbour interior) were represented by wave doublets. Table 4.3 shows the four conditions and the corresponding experimental tests for which the numerical results were obtained.

Test 5 corresponds to the case of highly reflecting breakwaters and interior boundaries (Phase 1) with waves propagating orthogonal to the breakwater ($\theta = 0°$) and a period T = 1.2 sec. Fig. 4.23 shows a comparison of the diffraction coefficient contours in the region behind the breakwater. Unfortunately there seems to be little correlation between the numerical and experimental results. This is probably due to the difference in grid size used and to the shortcomings in the experiments as indicated in section 4.3.1.1. For the experimental model a grid of 8 x 7 points was used to create the contour plot, whereas for the numerical model a grid size of

20 x 30 was used. The fluid boundaries were all highly reflecting giving rise to standing waves and therefore a large number of contour intervals. Lack of resolution with the experimental grid may have caused the omission of many contour lines thus changing the superficial appearance of the plot. However on close examination of Fig. 4.23 it becomes apparent that, at any given point the actual values of the diffraction coefficients are similar on both plots while the contours take different routes due to the lack of precision.

Test 9 corresponds to the case of highly reflecting breakwaters and interior boundaries (Phase 2) with waves propagating orthogonal to the breakwater ($\theta = 0°$) and a period of 0.8 sec. Fig. 4.24 shows a comparison of the diffraction coefficient contours in the region behind the breakwater. The agreement between the experimental results and the numerical predictions is now generally good, with all of the important features of the wave field within the harbour being reproduced. The lack of resolution of the experimental grid may again have contributed to the omission of some contour lines.

Test 12 was for the case of highly reflecting breakwaters and interior boundaries (Phase 2) with waves propagating orthogonal to the breakwater ($\theta = 0°$) and a period of 1.2 sec. Fig. 4.25 shows a comparison of the diffraction coefficient contours in the region behind the breakwater. Agreement is generally quite good, with the numerical model underestimating the wave heights within the harbour. This may be due to radiating secondary waves generated at the breakwater tip as indicated by Pos and Kilner, 1987. The occurence of secondary waves has been described by Biesel (1963) who states that "any local surface pressure fluctuations of a given frequency will give rise to a circular wave of the same frequency and radiating energy in all directions."

Test 14 was for the case of highly reflecting breakwaters and interior boundaries (Phase 2) with waves propagating at an angle to the breakwater ($\theta = +30°$) and a period T = 0.8 sec. Fig. 4.26 shows a comparison of the diffraction coefficient contours in the region behind the breakwater. Agreement between the numerical and experimental contour plots is generally quite good, with the

numerical model underestimating the wave heights within the harbour. The lack of resolution of the experimental grid may again have caused the omission of some contour lines.

In all cases the wave heights decrease significantly in the shadow region. In general the wave heights within the harbour are slightly underpredicted. This phenomenon has been reported previously by Pos and Kilner, 1987 and may be due to radiating secondary waves as described earlier in this section.

Chapter 5
Conclusions & Recommendations

5.1 Conclusions

A numerical method developed by Isaacson and Baldwin (1991) for predicting the wave field in a harbour of constant depth and arbitrary shape which contains partially reflecting boundaries has been verified as predicting the wave field accurately. The approach used is based on linear diffraction theory and uses a wave doublet representation of the harbour boundaries.

Numerical results are presented for the wave field due to a specified incident wave train approaching a straight offshore breakwater, a semi-circular harbour with a pair of symmetrical protruding breakwaters, and a rectangular harbour with a pair of symmetrical protruding breakwaters. The wave field in the lee-side of the straight offshore breakwater predicted by the numerical model agrees closely with the exact solution. For the semi-circular harbour case, the boundaries were considered to be perfectly absorbing, and the numerical model predicts the wave field within the harbour realistically. For the rectangular harbour, cases which are considered include perfectly absorbing, perfectly reflecting and partially reflecting harbour boundaries. In all of these cases the numerical model predicts the wave field within the harbour realistically.

The numerical model using a doublet representation for both one-sided and two-sided fluid boundaries is compared to an experimental model for different wave period, incident wave direction, incident wave height, reflection coefficients of the harbour boundaries and reflection coefficients of the breakwaters. The agreement between the experimental results and the numerical predictions is generally good. As a rule the wave heights within the harbour are slightly underpredicted, while the wave heights outside the harbour are slightly overpredicted.

The numerical model gives an accurate and reliable means of predicting the wave field within a harbour of arbitrary shape with partially reflecting boundaries. It is relatively easy to use and a users guide is available to help in the execution of the program.

5.2 Recommendations for Further Study

The scope of the present study was limited to partially reflecting one-sided boundaries and fully reflecting two-sided boundaries. The obvious progression from here is to investigate the case of partially reflecting two-sided boundaries. Isaacson and Baldwin (1991) made initial efforts to extend their method to the case of two-sided partially reflecting boundaries with limited success. The closed form solution for wave scattering around a partially reflecting straight breakwater exhibited noticeable wave height reduction along the surface with reduced reflection coefficients. However when the numerical method was applied the results exhibited a discontinuity in the velocity potential at the breakwater tip and convergence was not apparent. Research into this area would be another step along the road towards a numerical model which realistically predicts the wave field within an arbitrarily shaped harbour.

Bibliography

Beisel, F. 1963. "Radiating Second-Order Phenomena in Gravity Waves". *Recent Research in Coastal Hydraulics,* International Association of Hydraulic Research, 10th Congress, London, England, Vol. 1, pp. 197-203.

Berkhoff, J.C.W., 1976. "Mathematical models for Simple Harmonic Water Wave Diffraction and Refraction". *Delft Hydraulics Laboratory,* Rpt.No. 168.

Blue, F.L. and Johnson, J.W., 1949. "Diffraction of Water Waves Passing Through a Breakwater Gap". *Transactions of the American Geophysical Union,* Vol. 30, pp. 705-718.

Chen, H.S. and Mei, C.C., 1974. "Oscillations and Wave Forces in a Man-Made Harbour in the Open Sea". *Proceedings of the 10th Symposium on Naval Hydrodynamics,* Cambridge, Mass., pp. 573-596.

Garrett, C.J.C., 1970. "Bottomless Harbours". *Journal of Fluid Mechanics,* Vol. 43, pp. 432-449.

Harms, V.W., 1979. "Diffraction of Water Waves by Isolated Structures". *Journal of the Waterway, Port, Coastal and Ocean Division,* ASCE, Vol. 10 (WW2), pp. 131-147.

Hess, J.L., 1990. "Panel Methods in Computational Fluid Dynamics". *Annual Review of Fluid Mechanics,* Vol. 22, pp. 255-274.

Hunt, B., 1980. "The Mathematical Basis and the Numerical Principals of the Boundary Intregral Method for Incompressible Flows Over 3-D Aerodynamic Configurations", In *Numerical Methods in Applied Fluid Dynamics,* ed.B.Hunt, Academic Press, pp. 49-135.

Hwang, L.S. and Tuck, E.O., 1970. "On Oscillations of Harbours of Arbitrary Shape". *Journal of Fluid Mechanics,* Vol. 42, pp. 447-464.

Isaacson, M. 1991. "Measurement of Regular Wave Reflection", *Journal of the Waterway, Port, Coastal and Ocean Engineering,* ASCE, Vol. 117, No. 6, pp. 553-569.

Isaacson, M. and Qu, S., 1990. "Waves in a Harbour with Partially Reflecting Boundaries". *Coastal Engineering,* Vol. 14 , pp. 193-214.

Isaacson, M. and Baldwin, J., 1991. "Numerical Prediction of Wave Diffraction using a Doublet Distribution". *Coastal/Ocean Engineering Report*, Department of Civil Engineering, University of British Columbia, Vancouver, Canada.

Isaacson, M. and Baldwin, J., 1991. "Numerical Prediction of Wave Diffraction using a Doublet Distribution". *Proceedings of the Tenth Annual Conference of the Canadian Society for Civil Engineering*, Vancouver, British Columbia, Canada, pp. 76-85.

Johnson, J.W., 1951. "Generalized Wave Diffraction Diagrams". *Proceedings of the 2nd International Conference on Coastal Engineering*, Houston, Texas, pp. 6-23.

Lamb, H., 1932. "Hydrodynamics", Cambridge University Press, Cambridge.

Lee, J-J., 1971. "Wave induced Oscillations in harbours of Arbitrary Geometry". *Journal of Fluid Mechanics*, Vol. 45, pp 375-394.

Mattoli, F. and Tinti, S., 1979. "Discretization of the Harbour Reasonance Problem". *Journal of the Waterway, port, Coastal and Ocean Division*, ASCE, Vol. 105 (WW4), pp. 464-469.

Mei, C.C., 1978. "Numerical Methods in Water Wave Diffraction and Radiation". *Annual Review of Fluid Mechanics*, Vol. 10, pp. 393-416.

Memos, C.D., 1980. "Water Waves Diffracted by Two Breakwaters". *Journal of Hydraulic Research*, Vol. 18, No. 4, pp. 343-357.

Miles, J.W. and Munk, W.H., 1961. "Harbour Paradox". *Journal of Waterway and Harbours Division*, ASCE, Vol. 87, pp. 111-130.

Penny, W.G. and Price, A.T., 1952. "The Diffraction Theory of Sea Waves by Breakwaters and the Shelter Afforded by Breakwaters". *Philosophical Transactions*, Royal Society, Series A, Vol. 244, London, pp. 236-253.

Pos, J.D. and Kilner, F.A., 1987. "Breakwater Gap Diffraction: An Experimental and Numerical Study". *Journal of Waterway, Port, Coastal and Ocean Engineering*, ASCE, Vol. 113, No. 1, pp. 1-21.

Putman, J.A. and Arthur, R.S., 1948. "Diffraction of Water Waves by Breakwaters". *Transactions of the American Geophysical Union*, Vol. 29, pp. 481-490.

CERC, 1984. "Shore Protection Manual", 1, 4th Edition. Coastal Engineering Research Centre, U.S. Army Corps of Engineers, Vicksburg, Mississippi.

Sobey, R.J. and Johnson, T.L., 1986. "Diffraction Patterns near Narrow Breakwater Gaps". *Journal of Waterway, Port, Coastal and Ocean Engineering,* ASCE, Vol. 112, No. 4, pp 512-528.

Wiegel, R.L., 1962. "Diffraction of Waves by a Semi-infinite Breakwater". *Journal of the Hydraulics Division,* ASCE, Vol. 88, No.HY1, pp. 27-44.

Yeung, R.W., 1982. "Numerical Methods in Free-Surface Flow". *Annual Review of Fluid Mechanics,* Vol. 14, pp. 395-442.

Tables

Test run	θ (deg)	H (mm)	T (sec)	L (mm)	$\frac{d}{gT^2}$	$\frac{d}{L}$	K_r Breakwater	K_r Shoreline	Phase
1	+30	30	0.803	1,000	0.072	0.450	0.92	0.92	1
2	0	30	0.803	1,000	0.072	0.450	0.92	0.92	1
3	0	30	0.937	1,333	0.052	0.3375	0.92	0.92	1
4	0	30	1.068	1,666	0.040	0.270	0.92	0.92	1
5	0	30	1.200	2,000	0.032	0.225	0.92	0.92	1
6	0	15	0.803	1,000	0.072	0.450	0.92	0.92	1
7	-30	30	0.803	1,000	0.072	0.450	0.92	0.92	1
8	-30	30	0.803	1,000	0.072	0.450	0.92	0.21	2
9	0	30	0.803	1,000	0.072	0.450	0.92	0.21	2
10	0	30	0.937	1,333	0.052	0.3375	0.92	0.21	2
11	0	30	1.068	1,666	0.040	0.270	0.92	0.21	2
12	0	30	1.200	2,000	0.032	0.225	0.92	0.21	2
13	0	15	0.803	1,000	0.072	0.450	0.92	0.21	2
14	+30	30	0.803	1,000	0.072	0.450	0.92	0.21	2
15	+30	30	0.803	1,000	0.072	0.450	0.45	0.21	3
16	0	30	0.803	1,000	0.072	0.450	0.45	0.21	3
17	0	30	0.937	1,333	0.052	0.3375	0.45	0.21	3
18	0	30	1.068	1,666	0.040	0.270	0.45	0.21	3
19	0	30	1.200	2,000	0.032	0.225	0.45	0.21	3
20	0	15	0.803	1,000	0.072	0.450	0.45	0.21	3

Table 3.1   Wave conditions and reflection coefficients for each of the 20 test runs of the experimental model.

N	$\dfrac{F(N)}{F_{exact}}$
10	1.0360
20	1.0181
50	1.0071
100	1.0036
200	1.0020

Table 4.1   Effect of the number of segments N on the computed wave force on a vertical plate.

Material	K_r
Plywood	0.92
Rock (1:1.5)	0.45
Sand (1:2.5)	0.21

Table 4.2   Measured reflection coefficients for vertical plywood, rock at slope 1:1.5, and sand at a slope of 1:2.5 overlain with horsehair.

Test run	θ (deg)	T (sec)	L (m)	$\frac{d}{L}$	K_r Breakwater	K_r Shoreline
5	0	1.20	2.00	0.225	0.92	0.92
9	0	0.803	1.00	0.450	0.92	0.45
12	0	1.20	2.00	0.225	0.92	0.45
14	+30	0.803	1.00	0.450	0.92	0.45

Table 4.3   Wave conditions and reflection coefficients for the 4 test runs of the numerical model. (Note: Test number corresponds to that for the experimental model in Table 3.1)

Figures
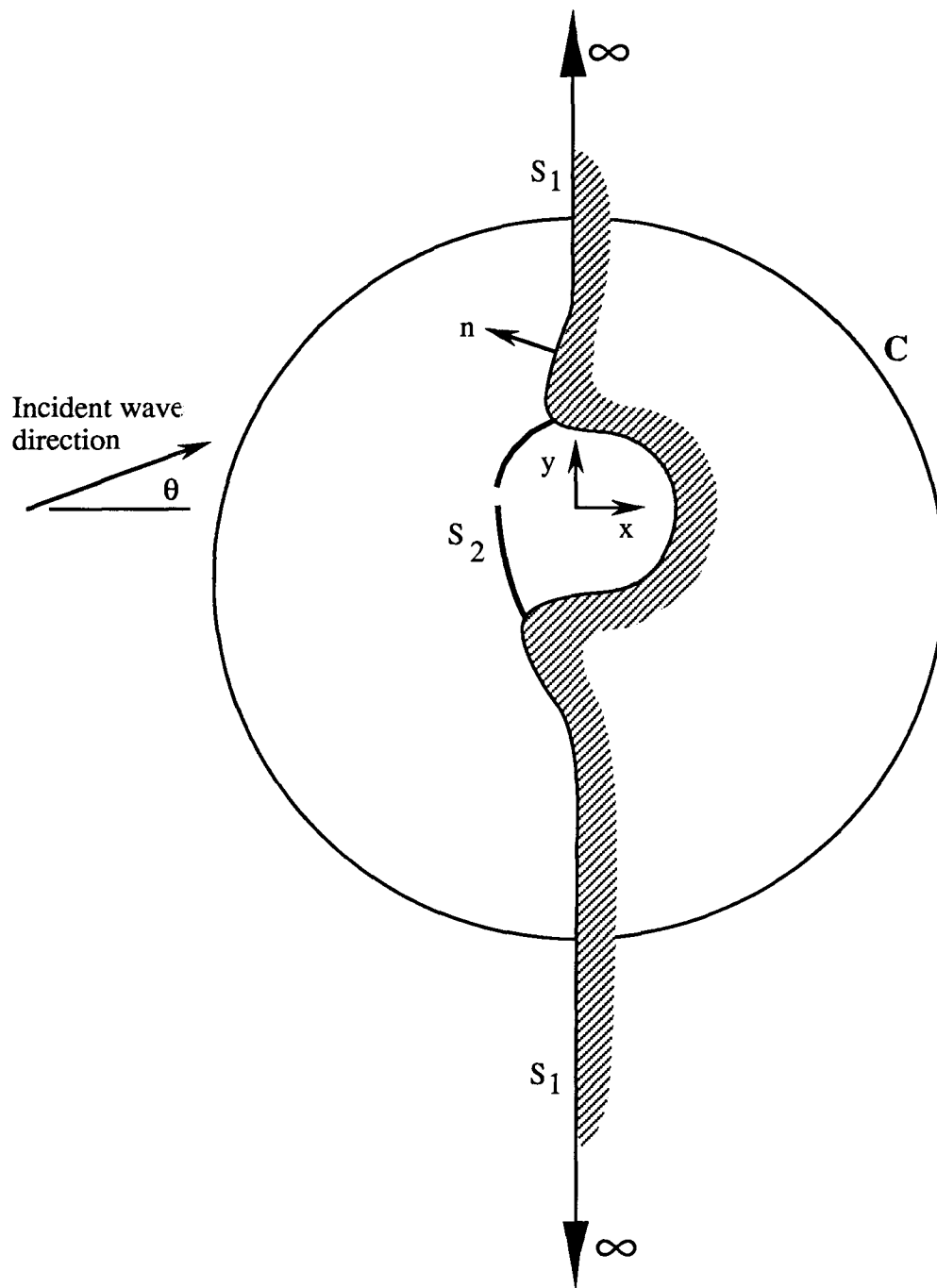
Figure 1.1   Definition sketch of general harbour.
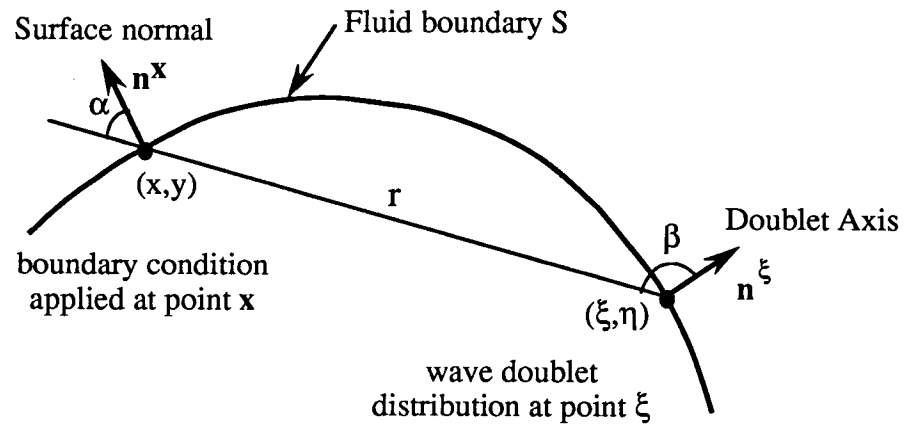
Figure 2.1   Geometry of Green's function representation .
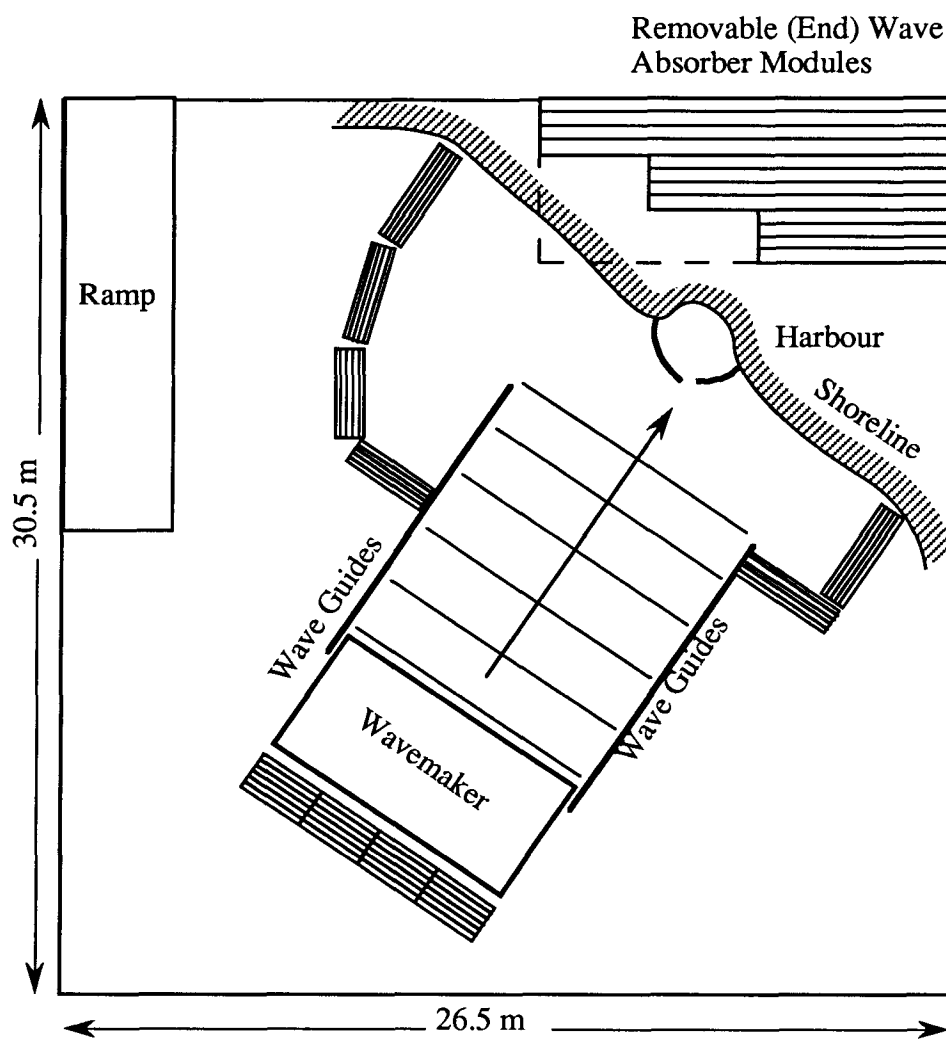
Figure 3.1   Sketch of the wave basin at BC Research.

43
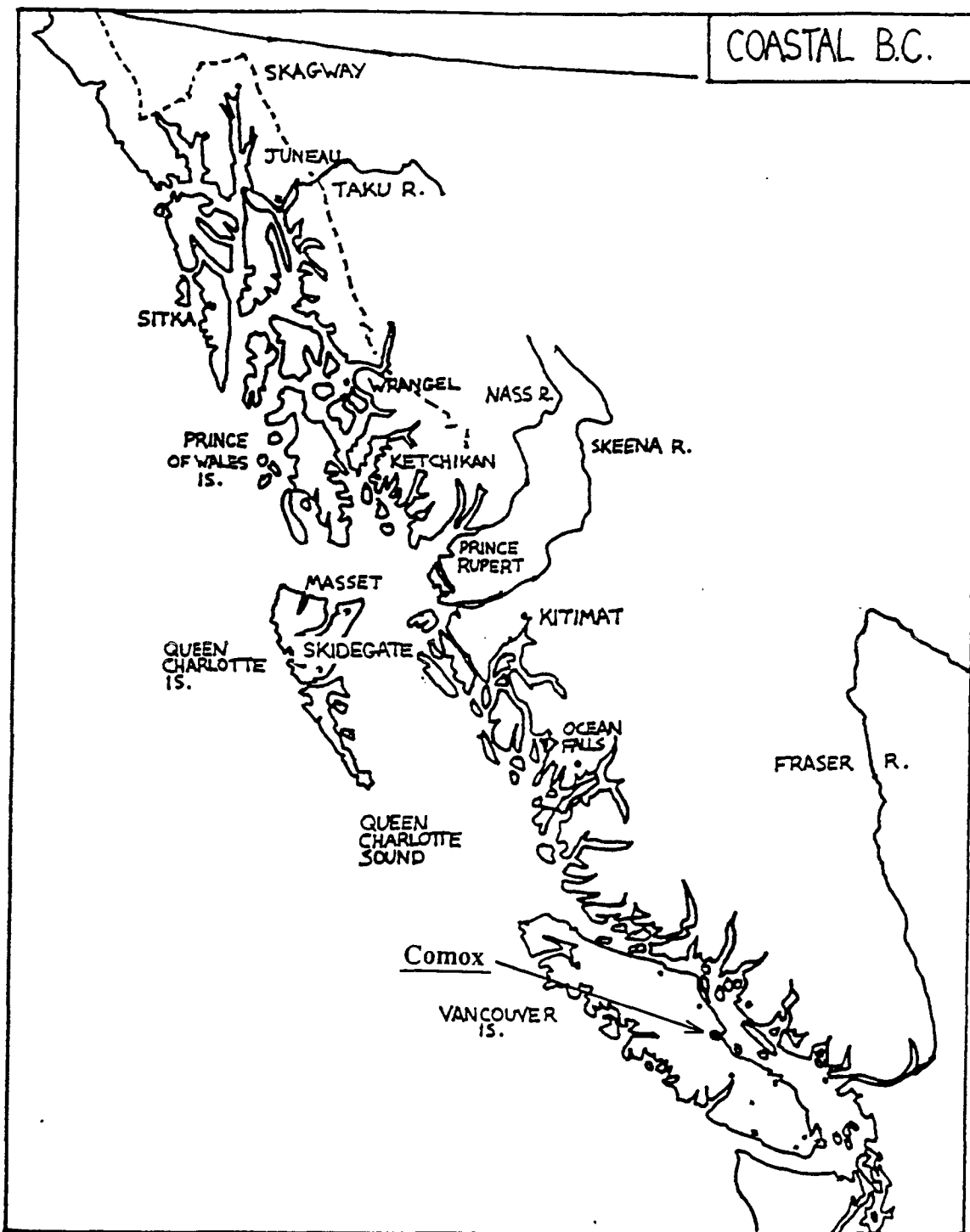
Figure 3.2   Location of Comox, BC.
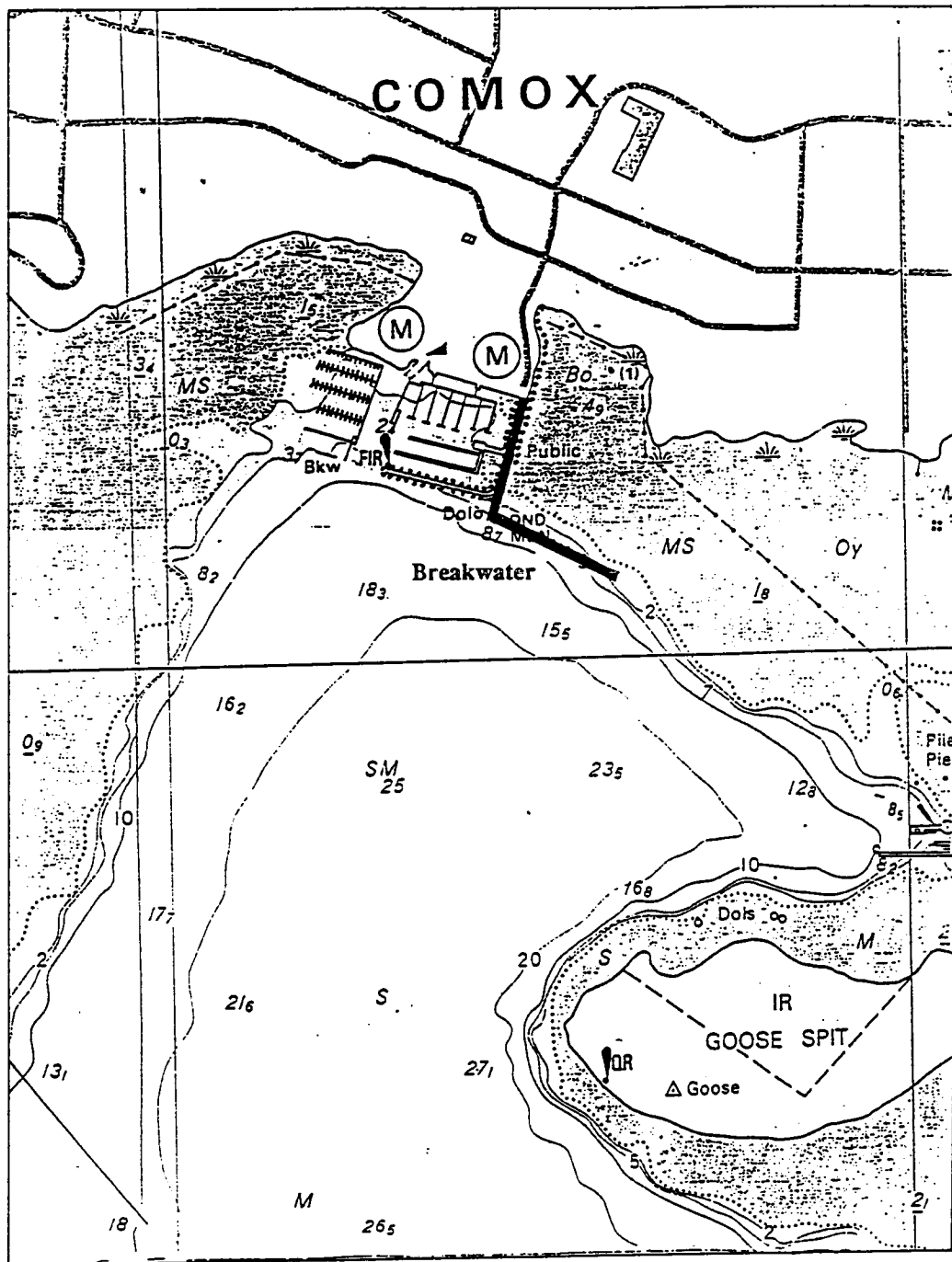
Figure 3.3   Details of Comox harbour.
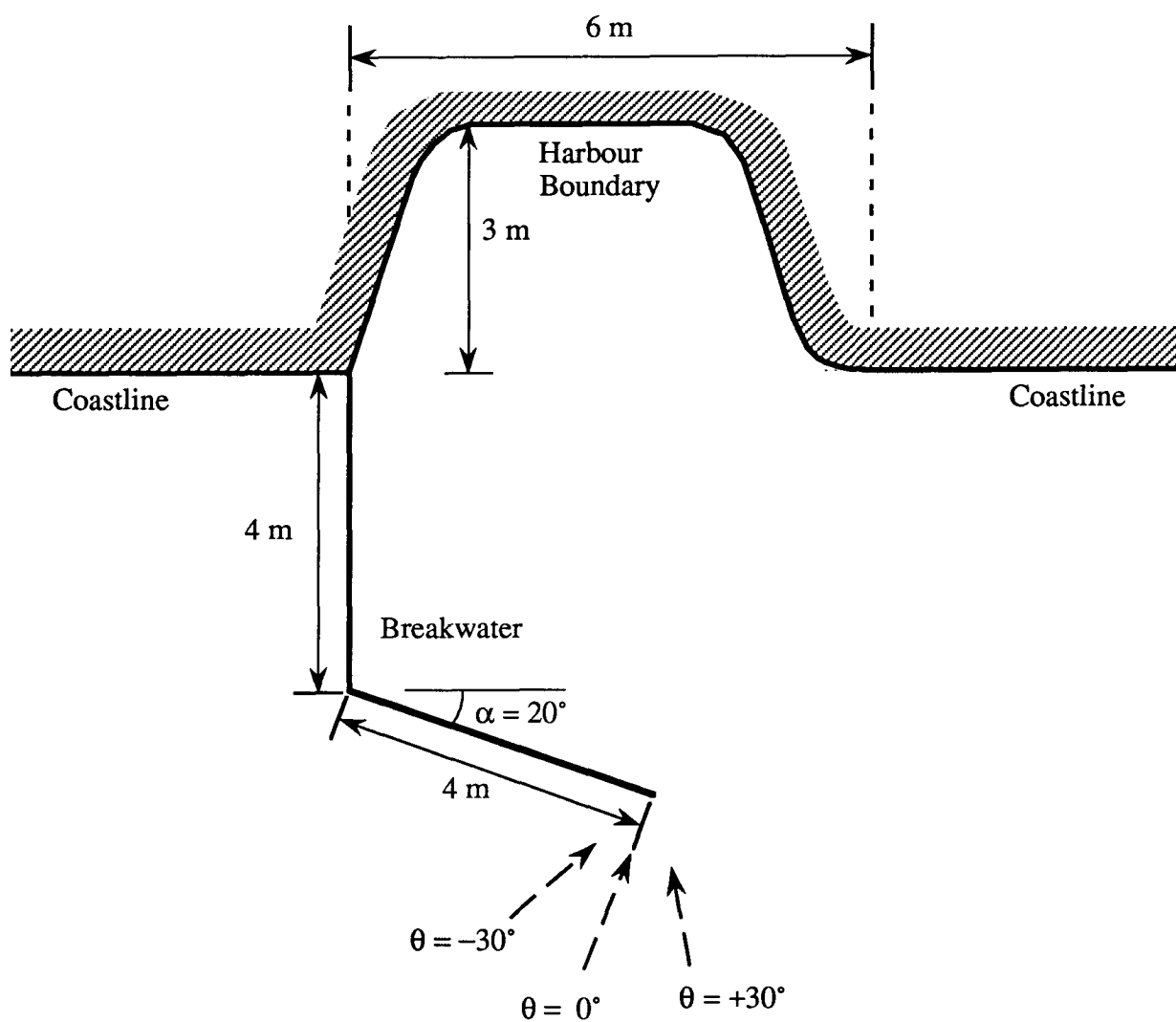
Figure 3.4   Sketch of the model harbour showing principal dimensions.
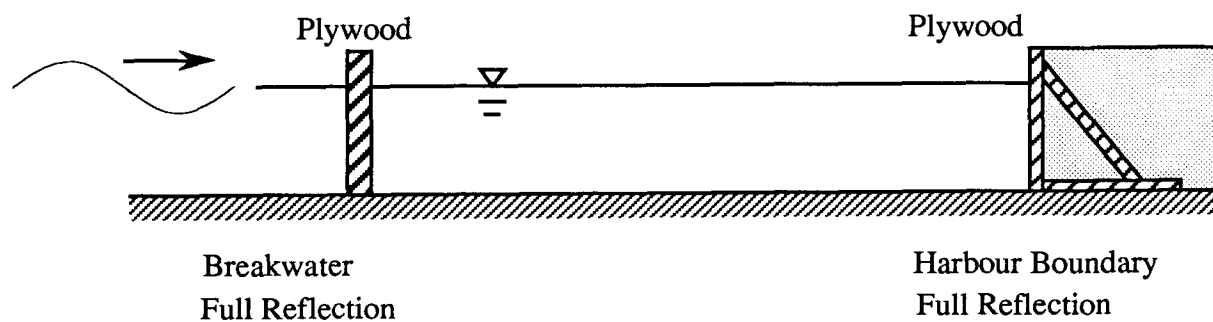
Phase 1
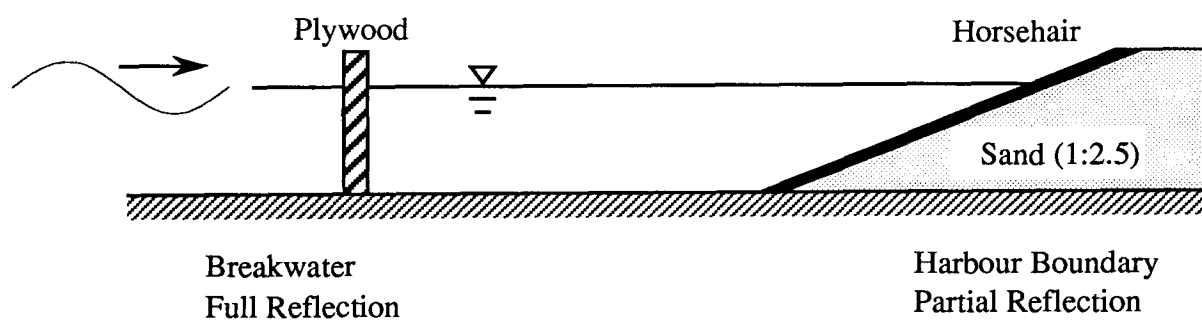
Phase 2
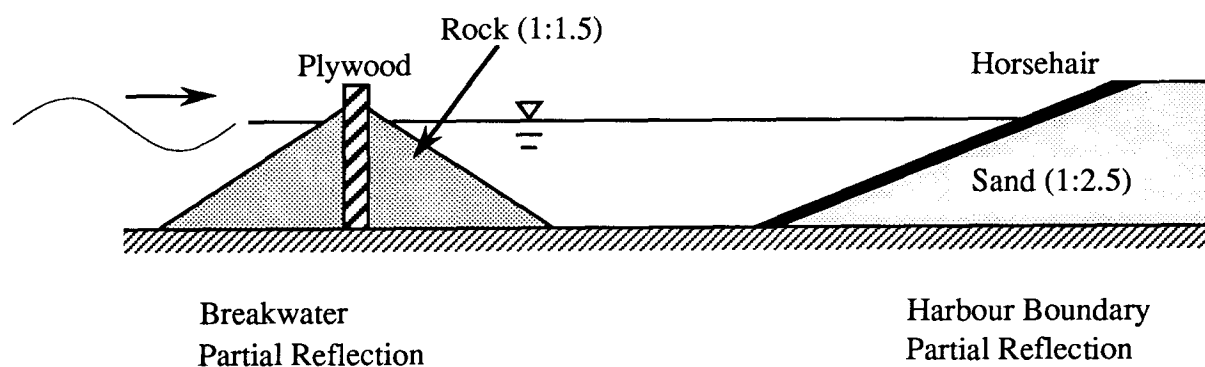
Phase 3

Figure 3.5   Sketch of the boundary configurations for the 3 Phases of the laboratory tests.
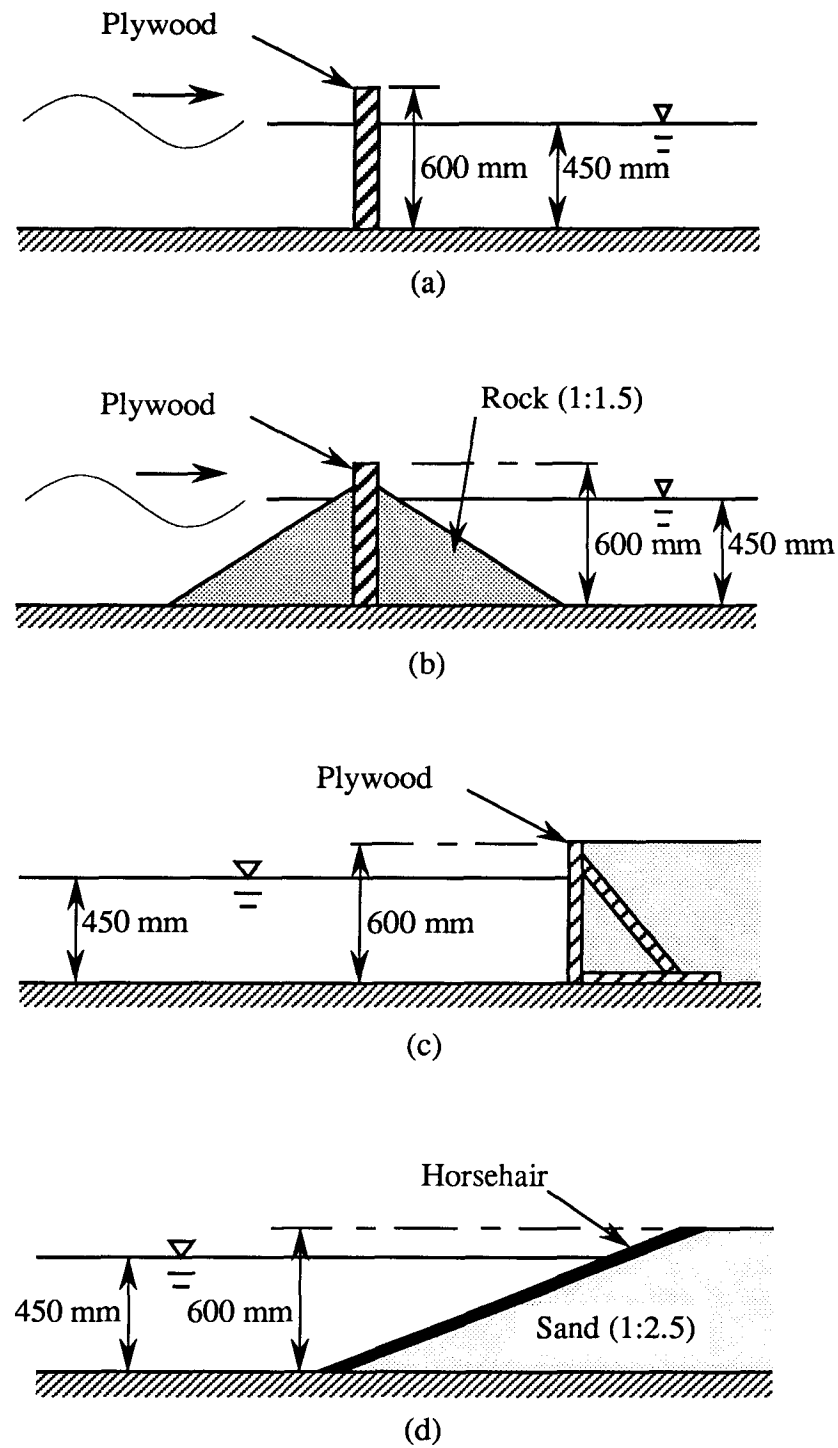
Figure 3.6   Dimensions of the and harbour boundaries. (a) breakwater for Phases 1 and 2, (b) breakwater for Phase 3, (c) harbour boundary for Phase 1, (d) harbour boundary for Phases 2 and 3.
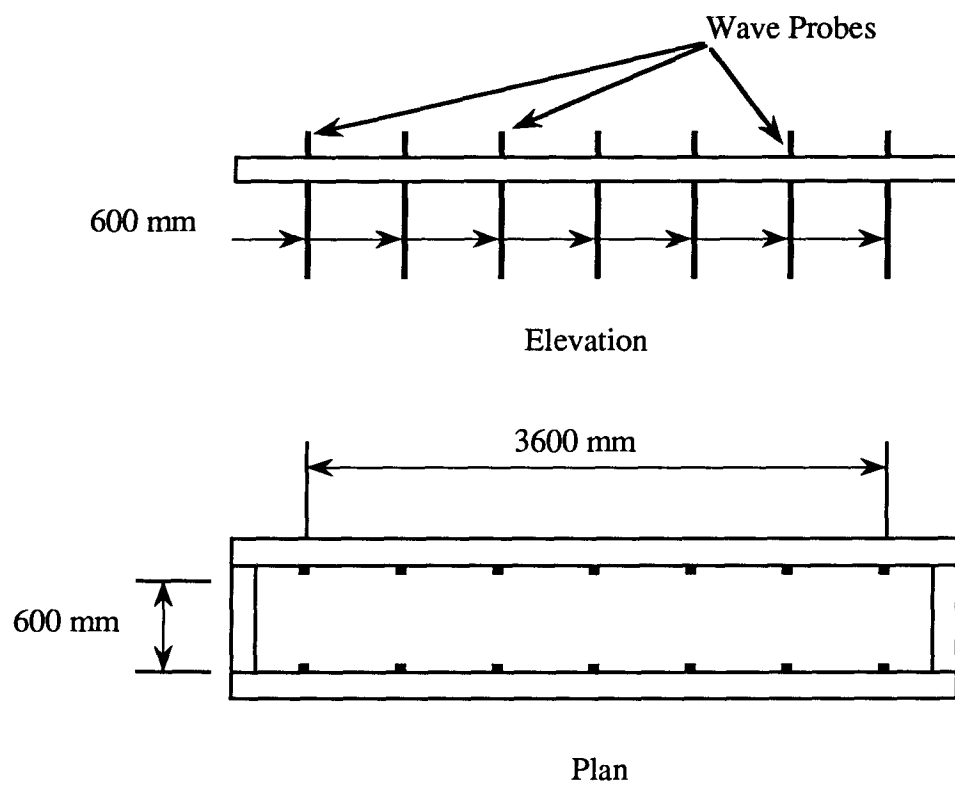
Figure 3.7   Sketch of the wave probe frame.
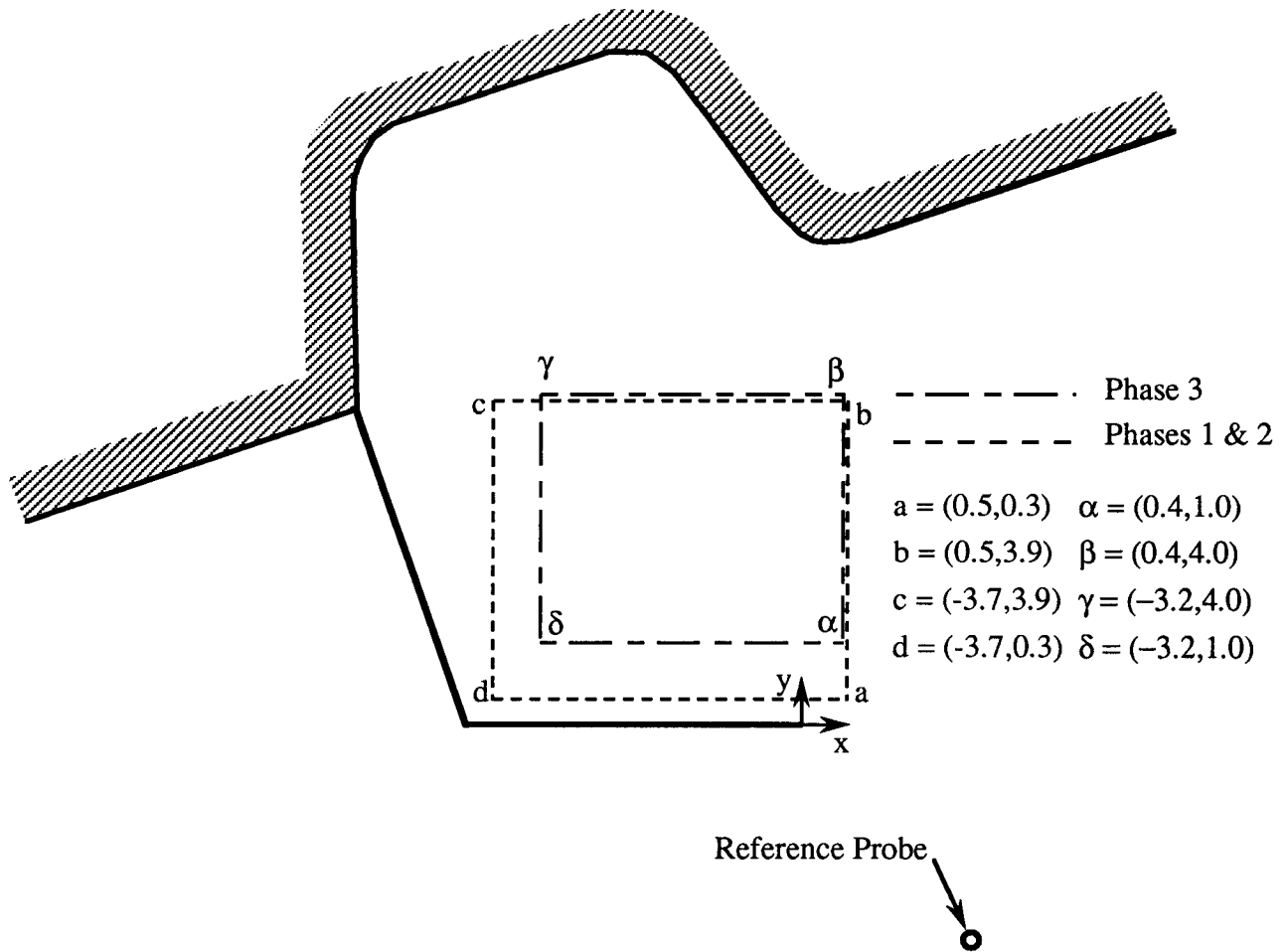
Figure 3.8　Location of the wave field measurements.
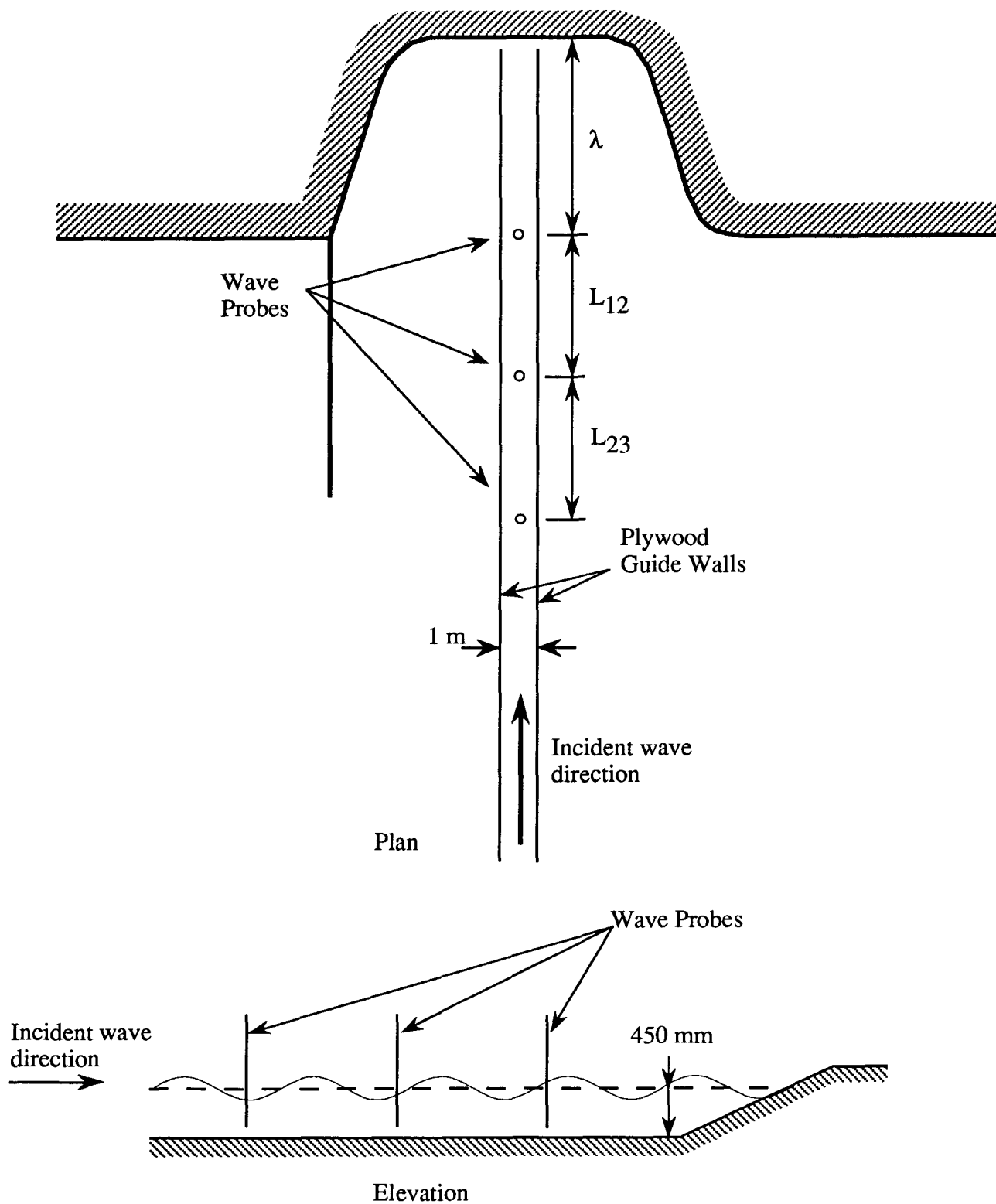
Figure 3.9   Sketch of experimental layout for reflection coefficient measurement.
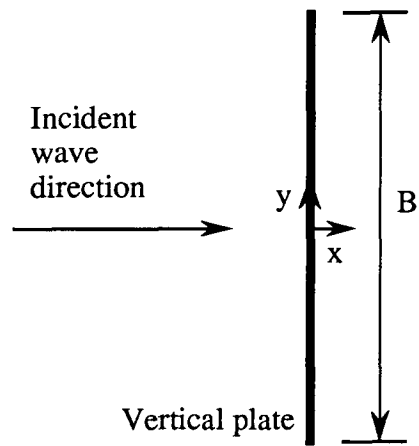
Figure 4.1   Rigid vertical plate used in the numerical example.
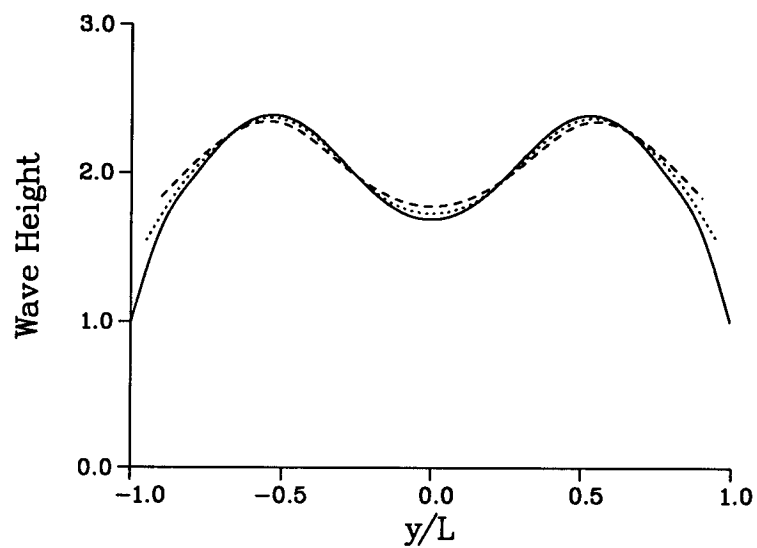
(a)
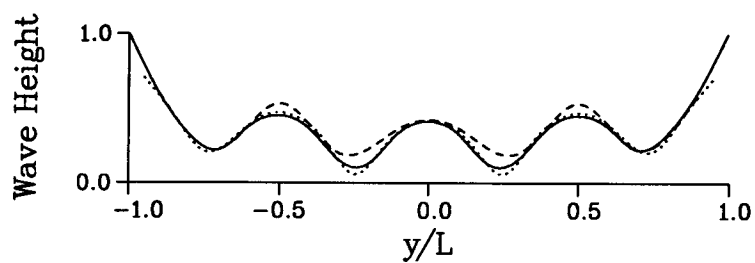
(b)

Figure 4.2 Wave height distribution along a straight offshore breakwater with B/L = 2.0, θ = 0°.
(a) upwave face, and (b) downwave face. ·········· N = 10, - - - - - - N = 20,
———— exact solution.
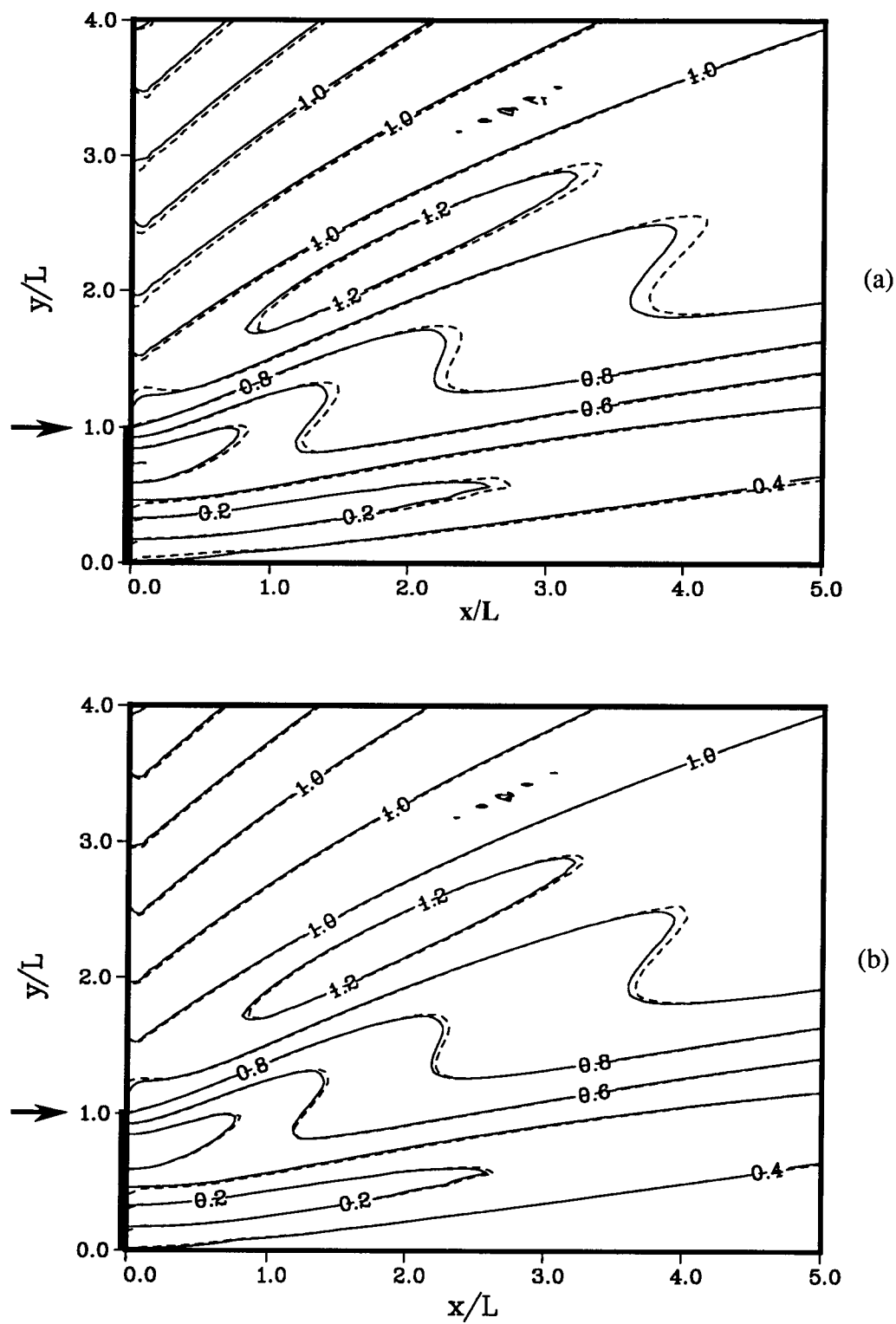
Figure 4.3   Diffraction coefficient contours in the vicinity of the offshore breakwater
                with B/L = 2.0, θ = 0°. ———— exact solution, ------- numerical solution.
                (a) N = 20, (b) N = 50.
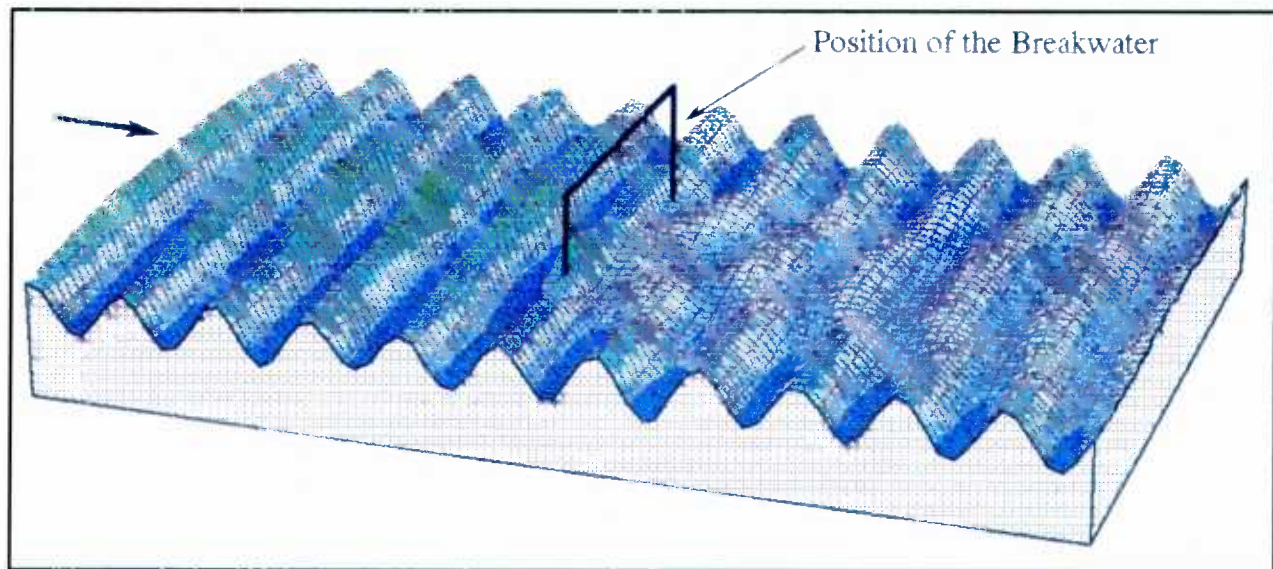
Figure 4.4   View of surface elevation (at t = 0) in the region of the offshore breakwater for B/L = 2.0 and θ = 0°.
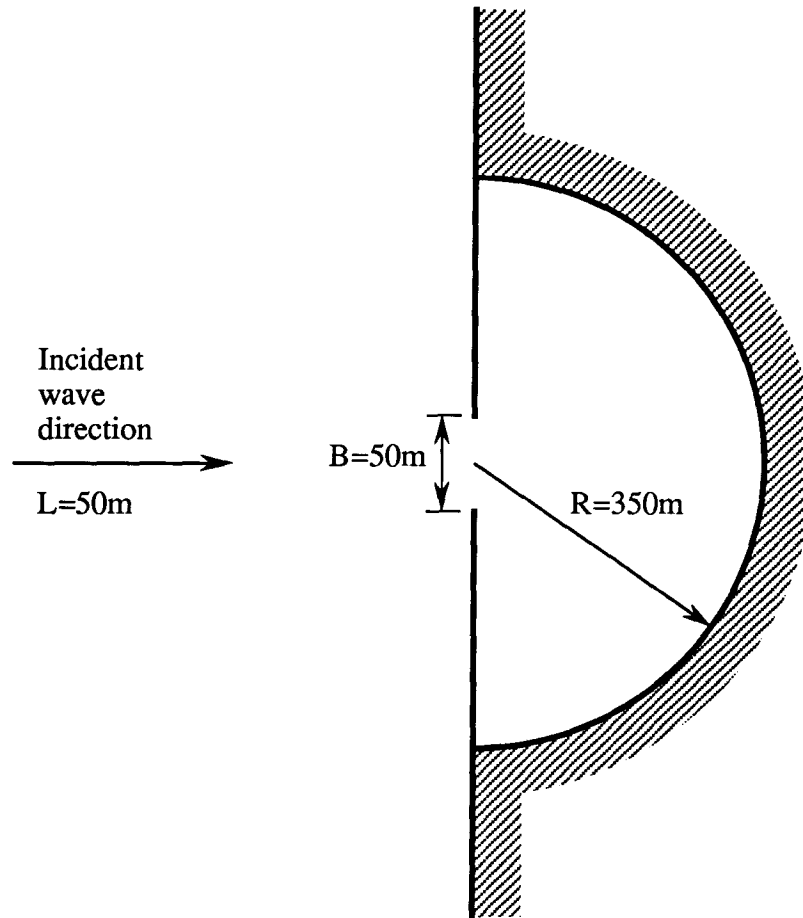
Figure 4.5   Sketch of the semi-circular harbour used as a numerical example.
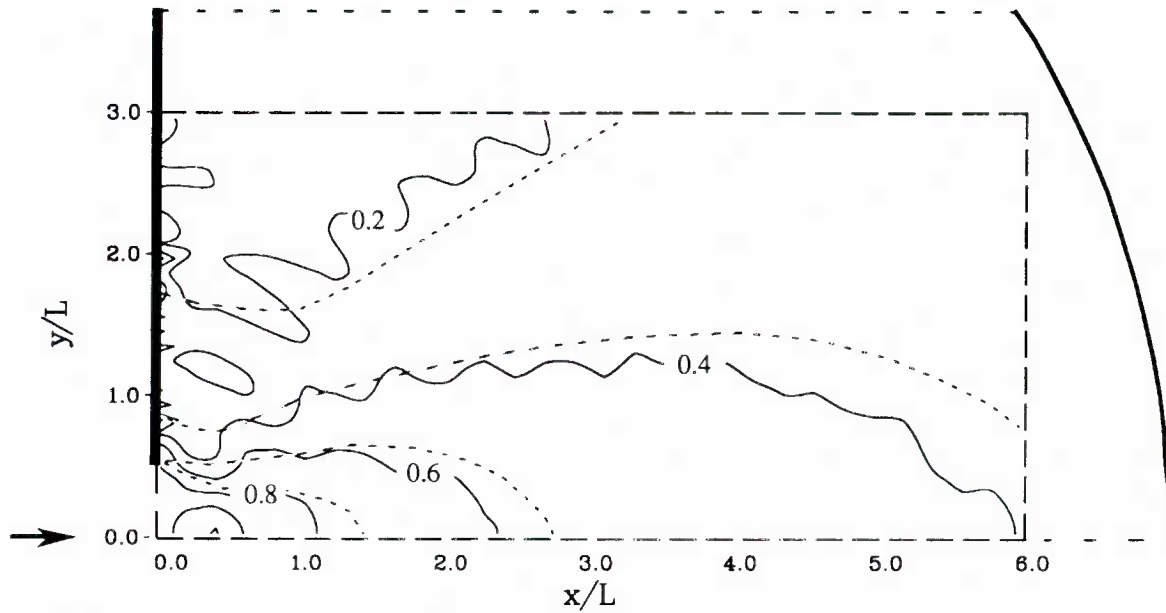
Figure 4.6 Diffraction coefficients in the vicinity of a breakwater gap with B/L = 1.0, θ = 0° and K$_r$ = 0. ------- numerical solution for semi-circular harbour, - - - - - exact solution for breakwater gap (Sobey and Johnson, 1986).
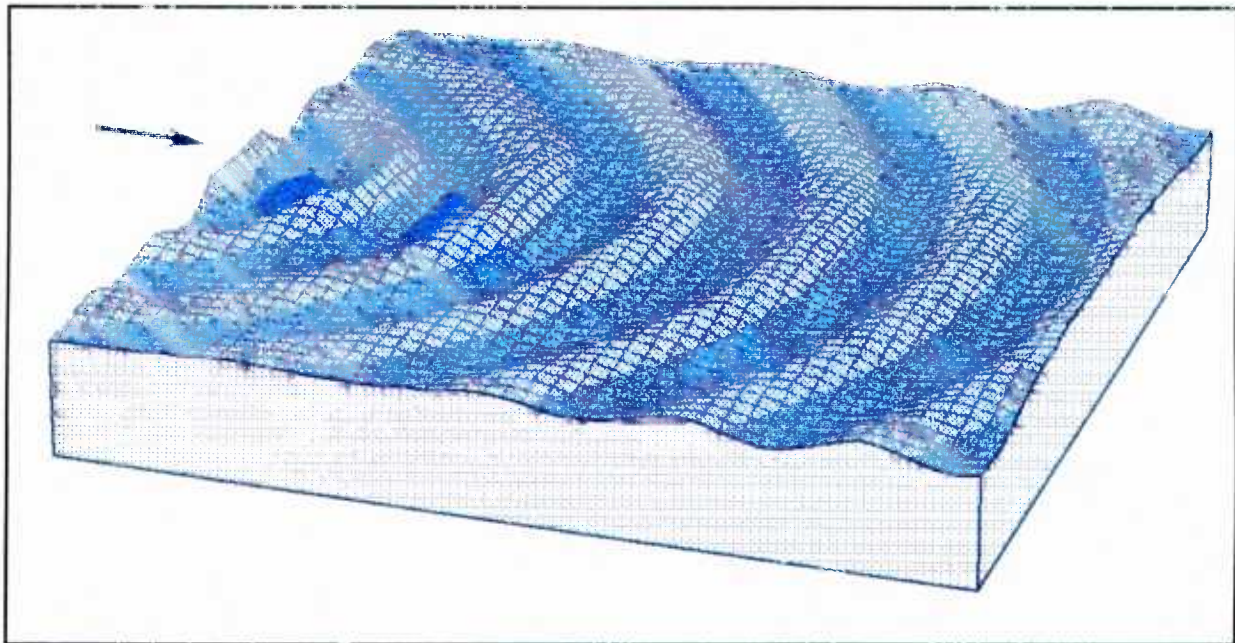
Figure 4.7 View of the surface elevation (at t = 0) in the region of the breakwater gap for the semi-circular harbour with B/L = 1.0, θ = 0° and K$_r$ = 0.
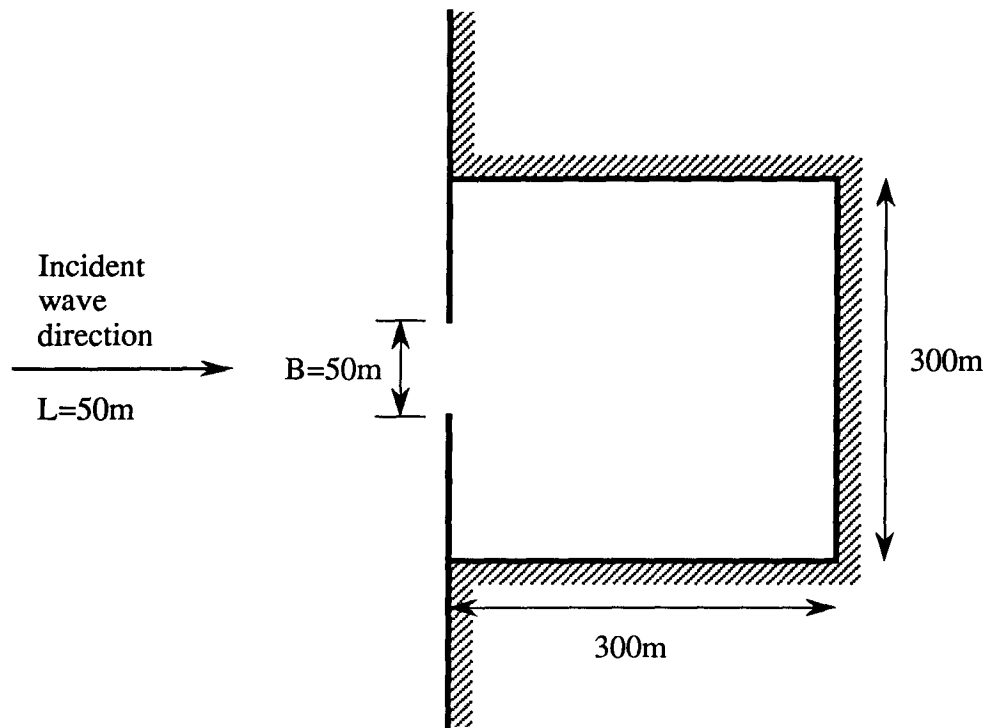
Figure 4.8   Rectangular harbour used as a numerical example.
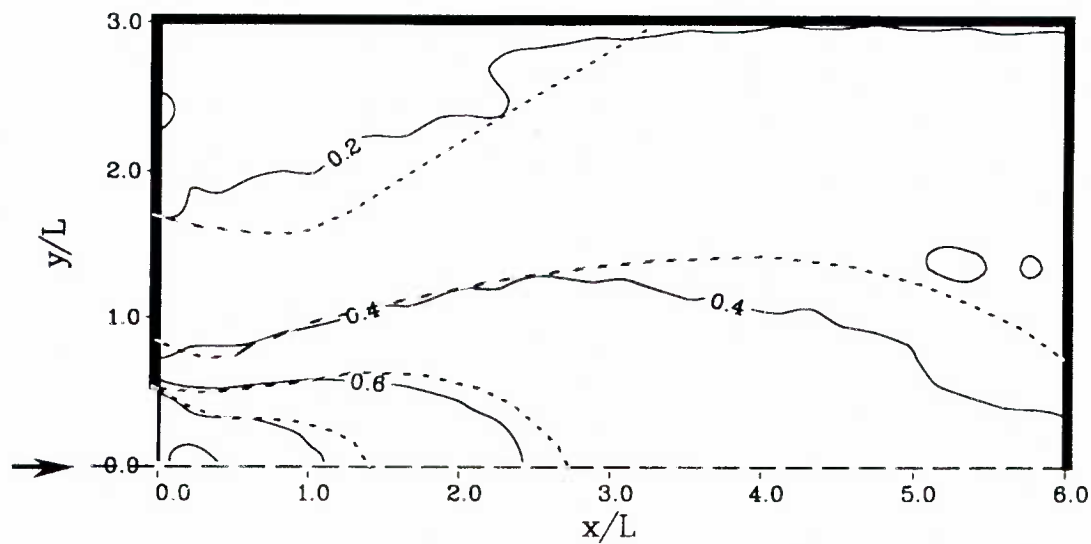
Figure 4.9   Diffraction coefficient contours within the rectangular harbour with B/L = 1.0, $\theta = 0°$ and $K_r = 0$. ———— numerical solution, - - - - - exact solution for breakwater gap (Sobey and Johnson, 1986).
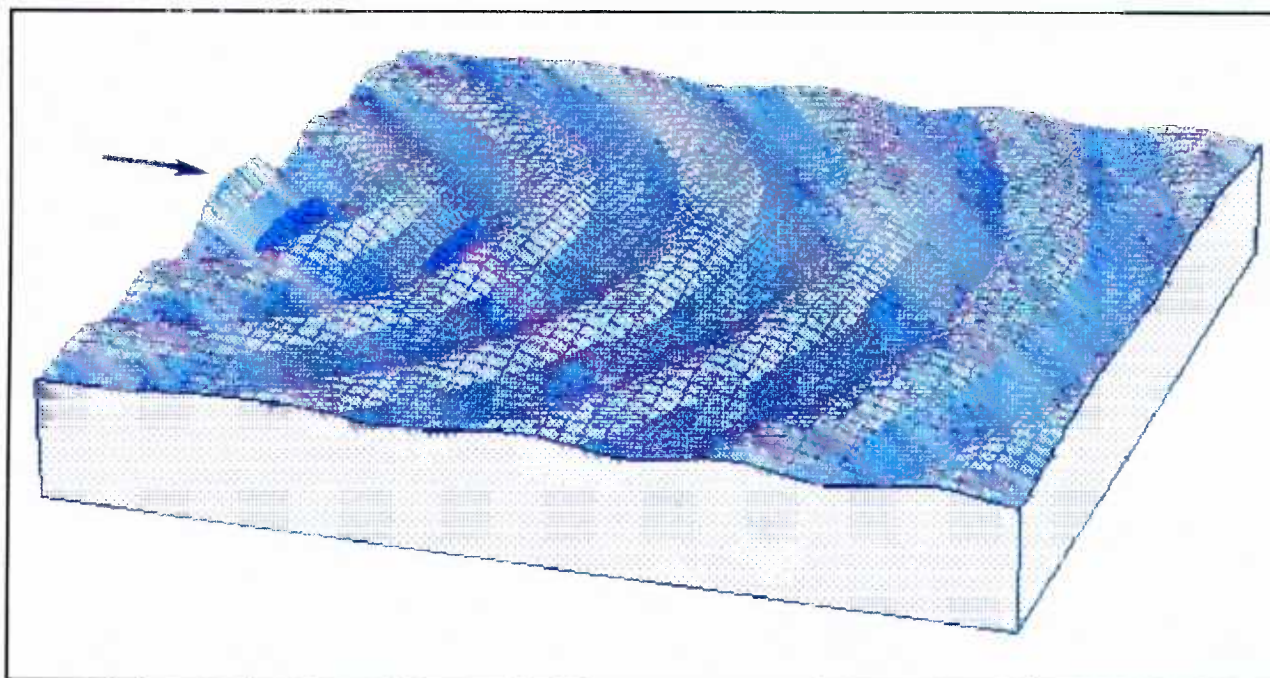
Figure 4.10   View of the surface elevation (at t = 0) for the rectangular harbour with B/L =1.0, $\theta = 0°$ and $K_r = 0$.
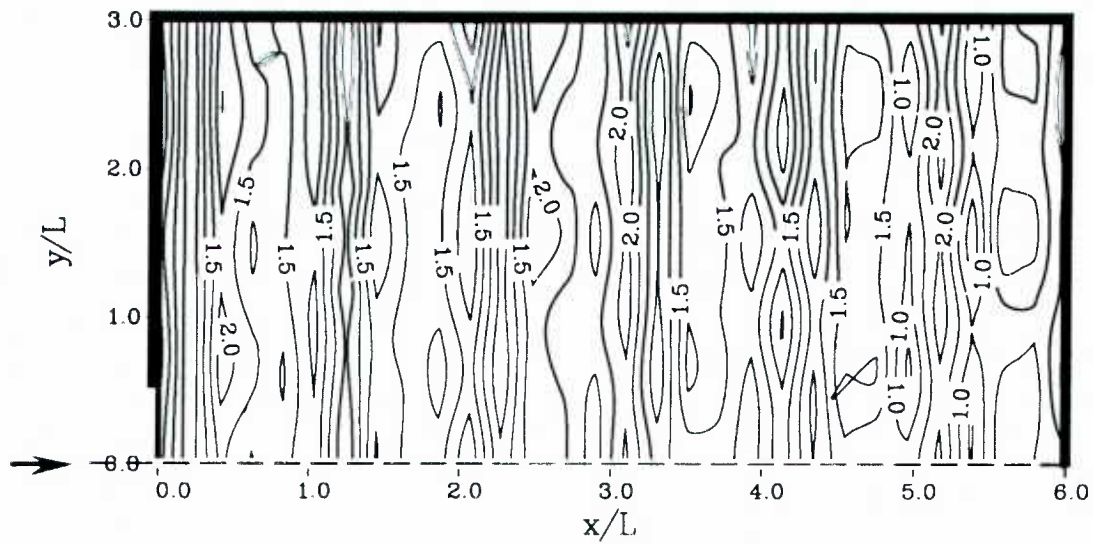
Figure 4.11   Diffraction coefficient contours within the rectangular harbour with B/L = 1.0, θ = 0° and K_r = 1.0.
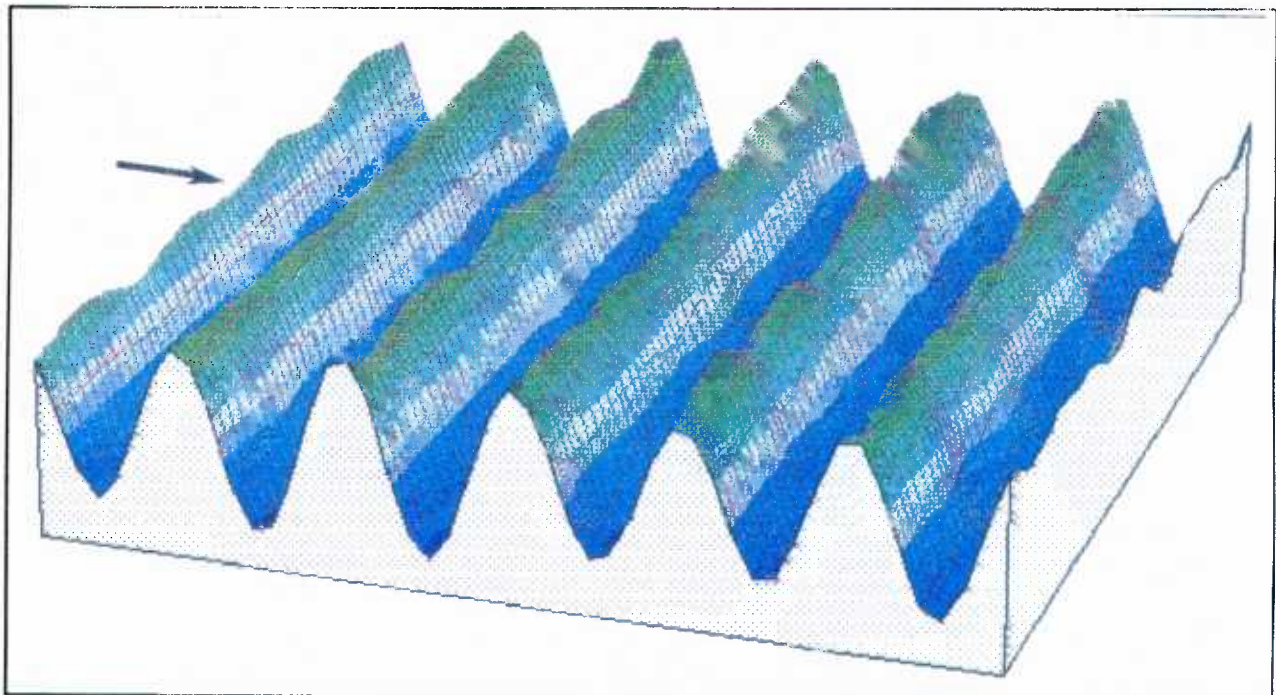
Figure 4.12   View of the surface elevation (at t = 0) for the rectangular harbour with B/L = 0, θ = 0, and K_r = 1.0.
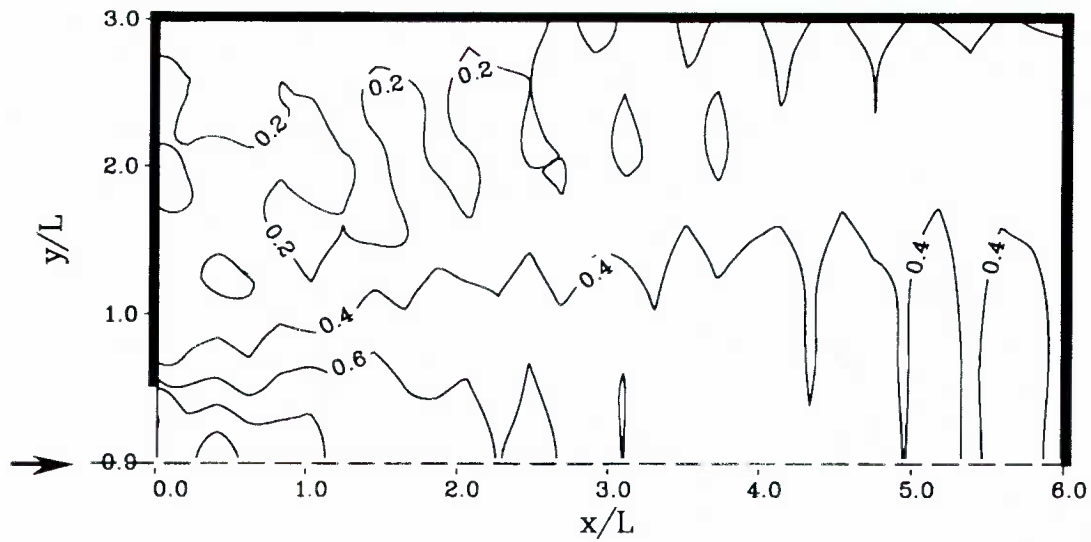
Figure 4.13   Diffraction coefficient contours within the rectangular harbour with B/L = 1.0, θ = 0° and K_r = 0.2.
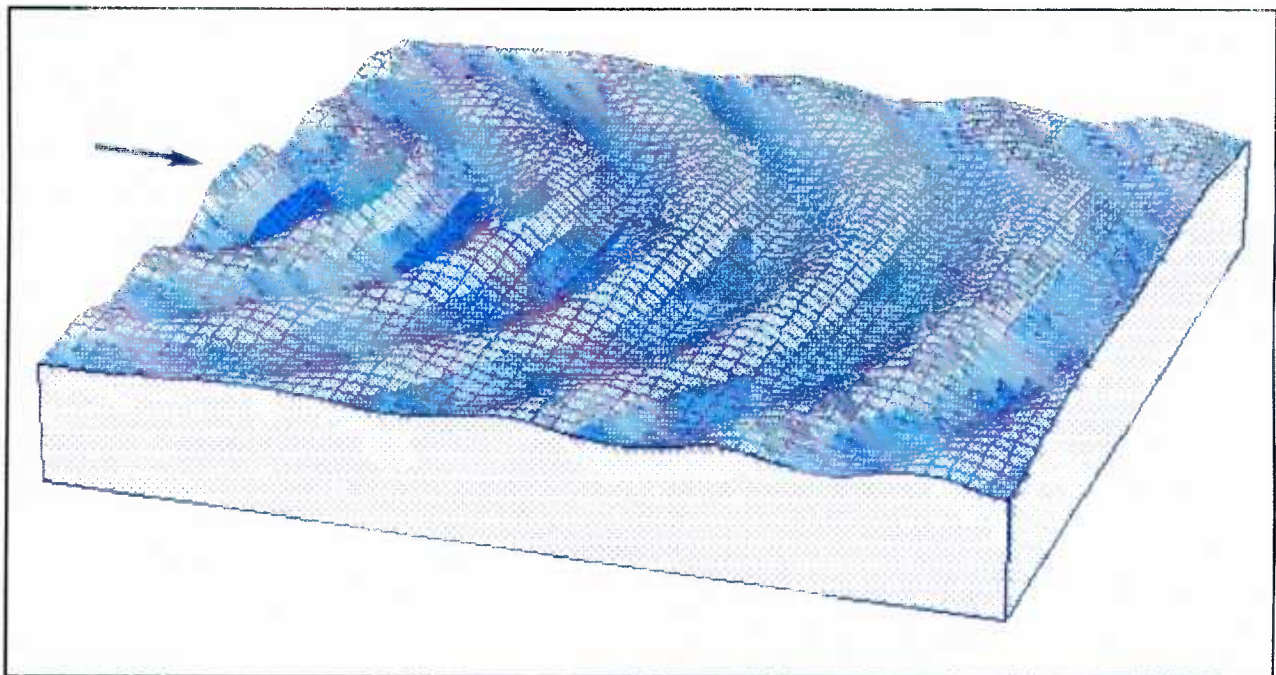
Figure 4.14   View of the surface elevation (at t = 0) for the rectangular harbour with B/L = 1.0, θ = 0°, and K_r = 0.2.
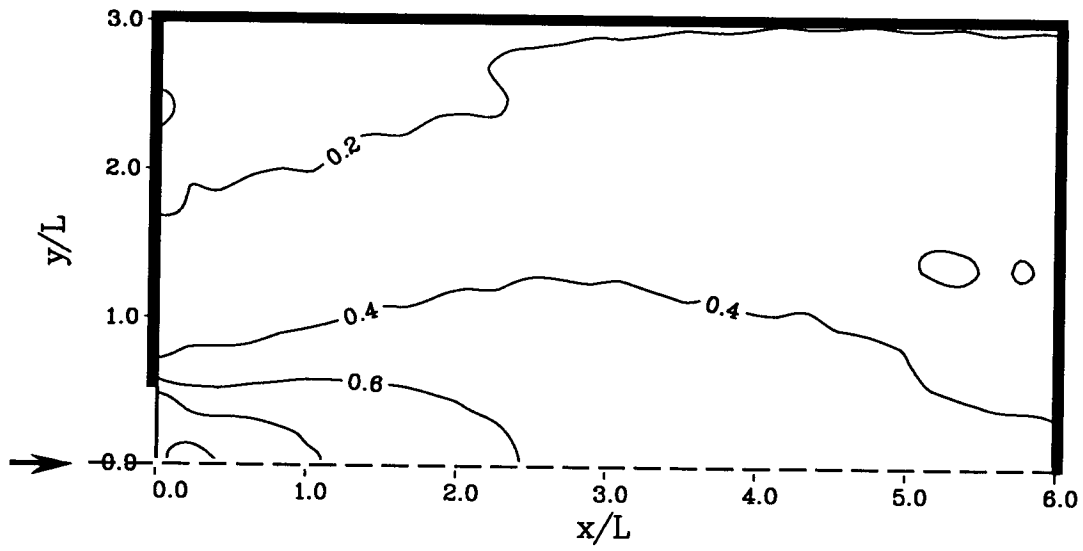
(a)
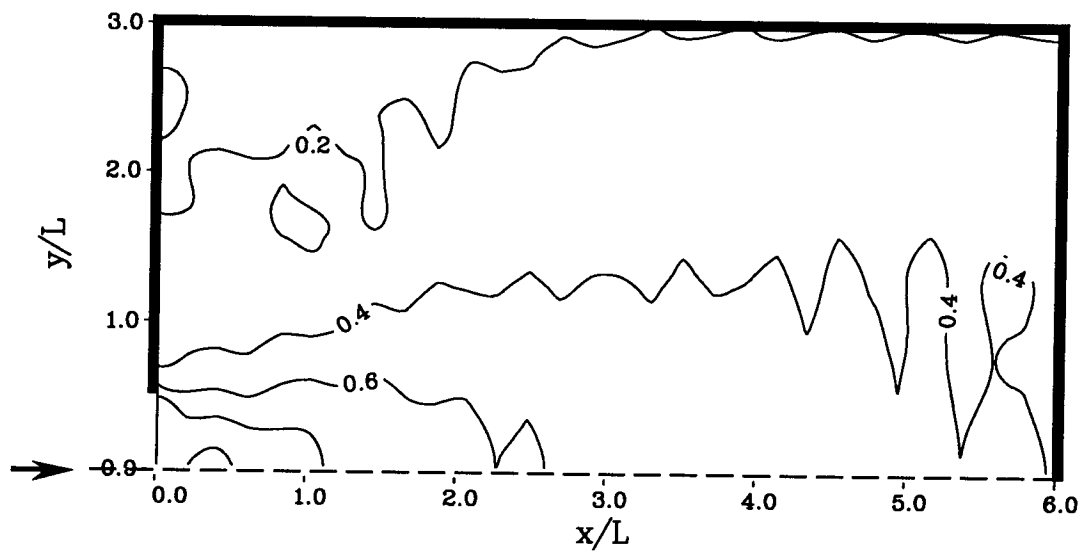
(b)

Figure 4.15   Diffraction coefficient contours within the rectangular harbour with B/L = 1.0,
θ = 0°. (a) K_r = 0.0, (b) K_r = 0.1 and (c) K_r = 0.2.
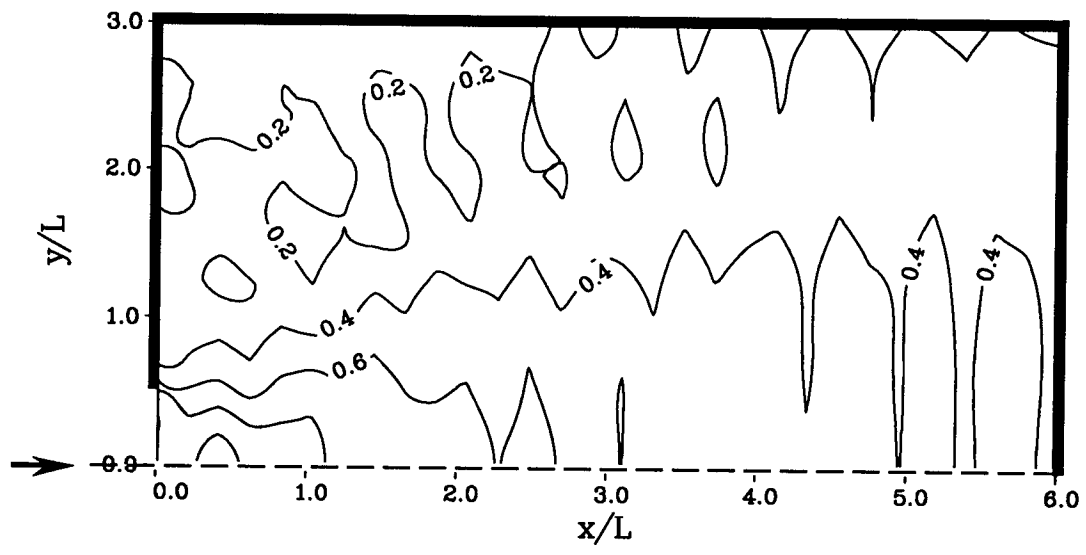
(c)

Figure 4.15   Continued.
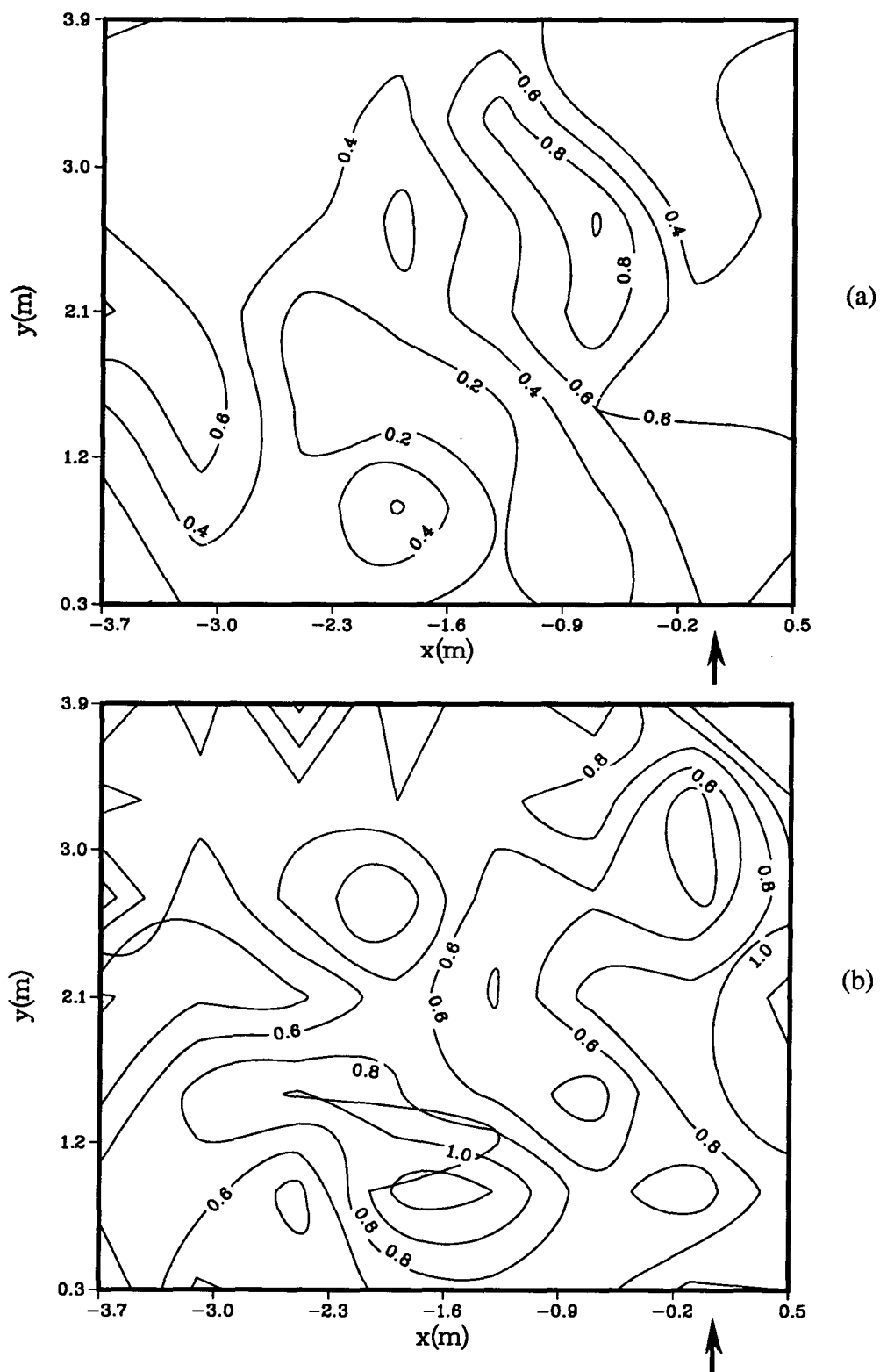
Figure 4.16   Diffraction coefficient contours for Phase 1 tests with θ = 0° and H = 30 mm
showing the effect of wave period. (a) T = 0.94 sec, (b) T = 1.07 sec,
(c) T = 1.2 sec.
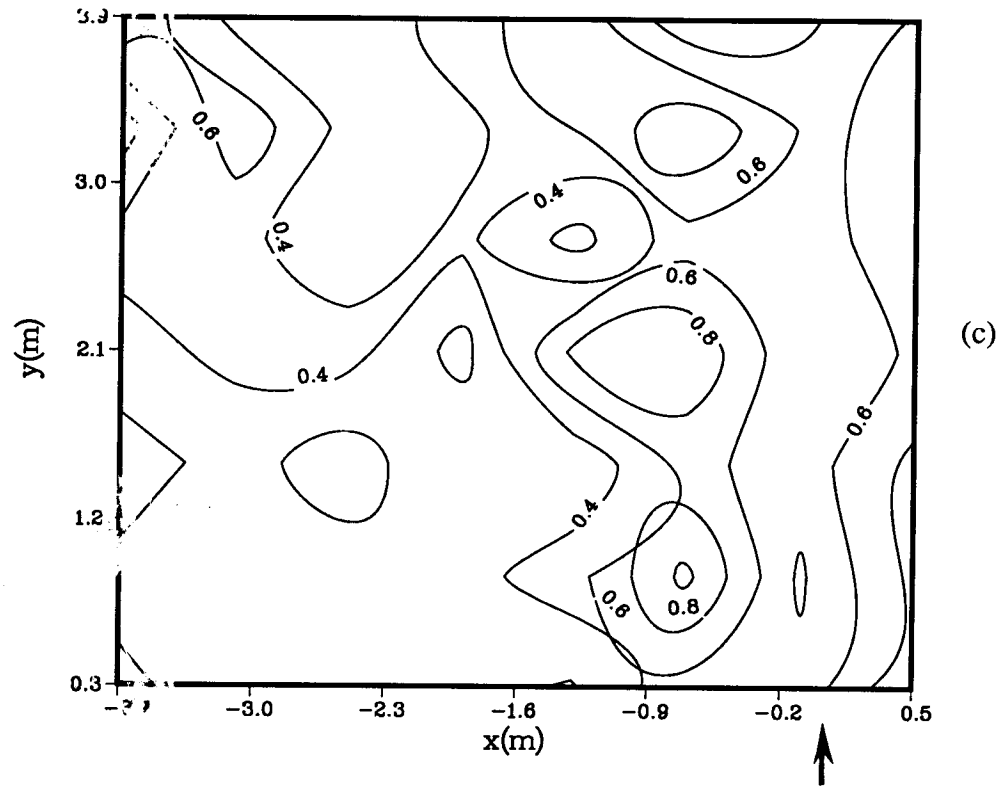
Figure 4.16   Continued.
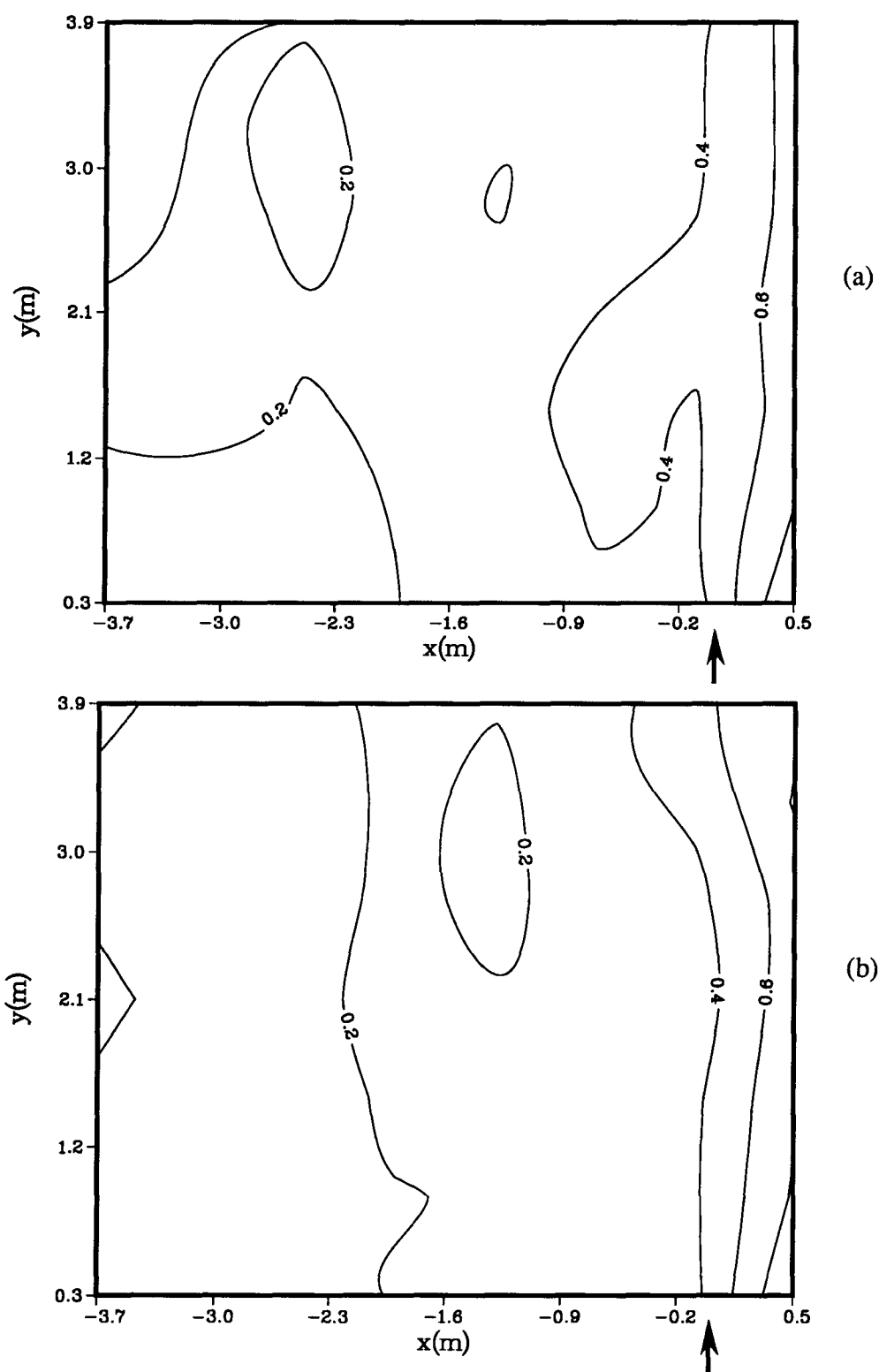
Figure 4.17   Diffraction coefficient contours for Phase 2 tests with θ = 0° and H = 30 mm
showing the effect of wave period. (a) T = 0.8 sec, (b) T = 0.94 sec,
(c) T = 1.04 sec, (d) T = 1.2 sec.
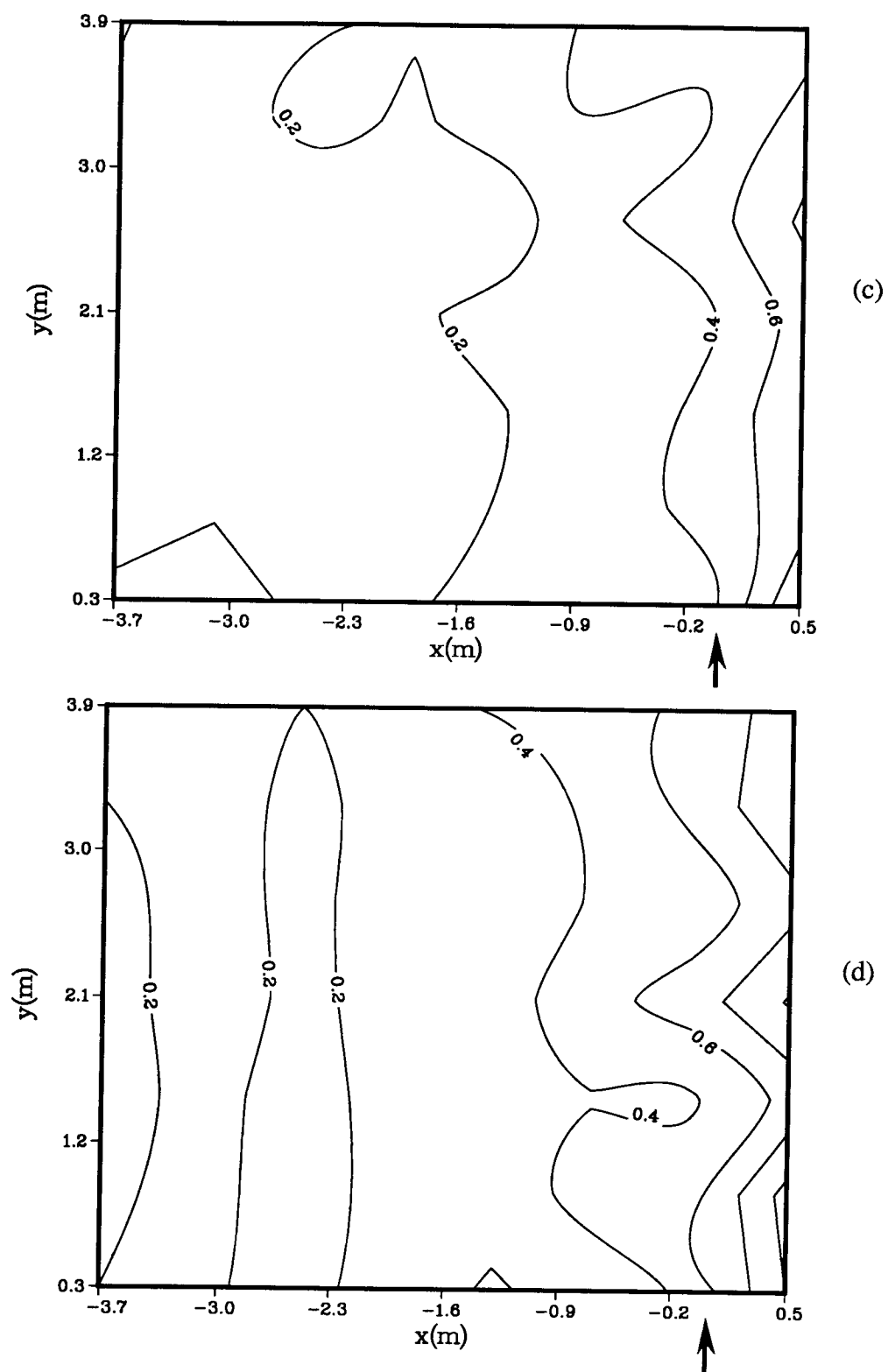
Figure 4.17   Continued.
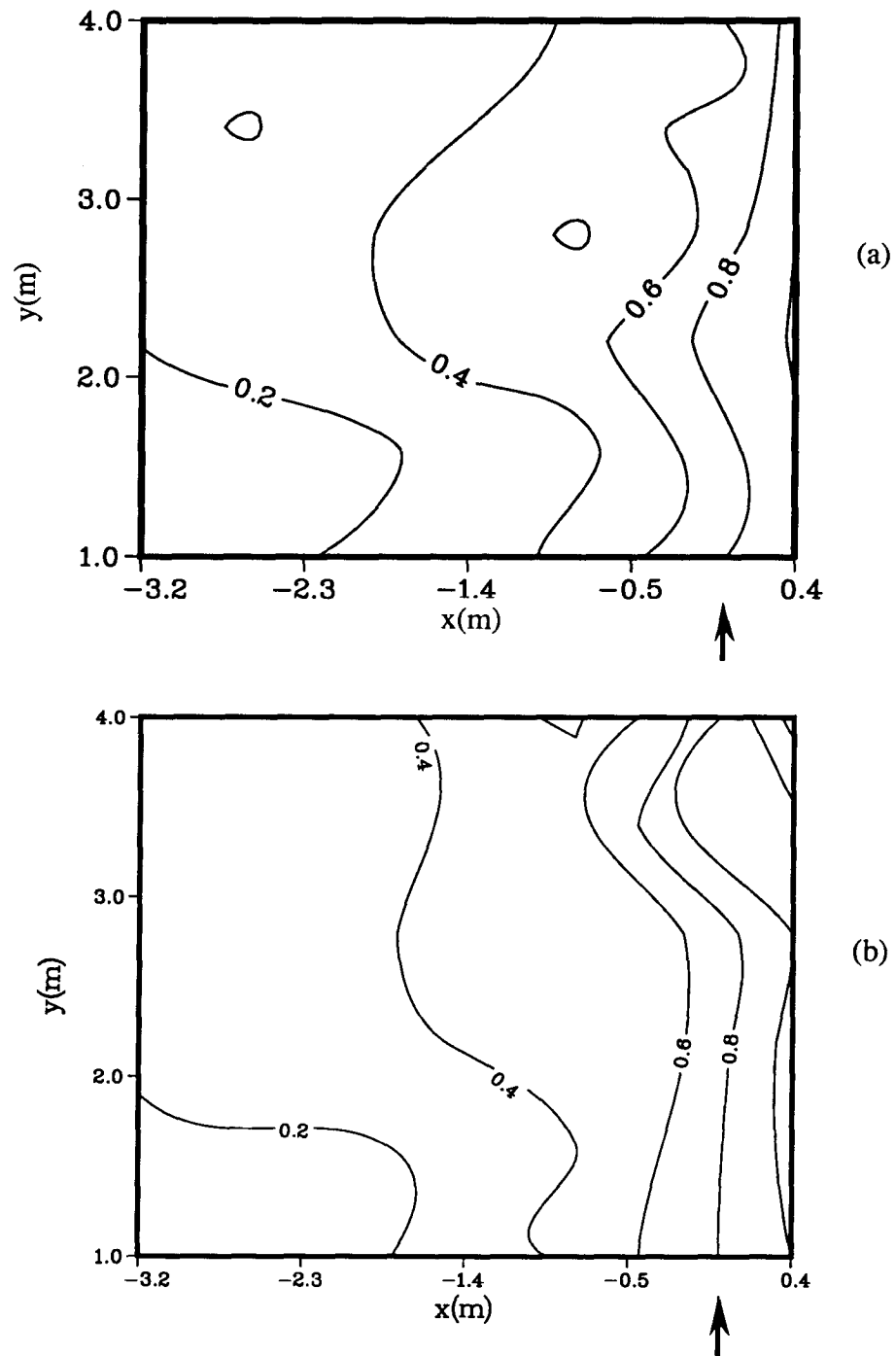
Figure 4.18   Diffraction coefficient contours for Phase 3 tests with θ = 0° and H = 30 mm showing the effect of wave period. (a) T = 0.8 sec, (b) T = 0.94 sec, (c) T = 1.04 sec, (d) T = 1.2 sec.

(c)

(d)
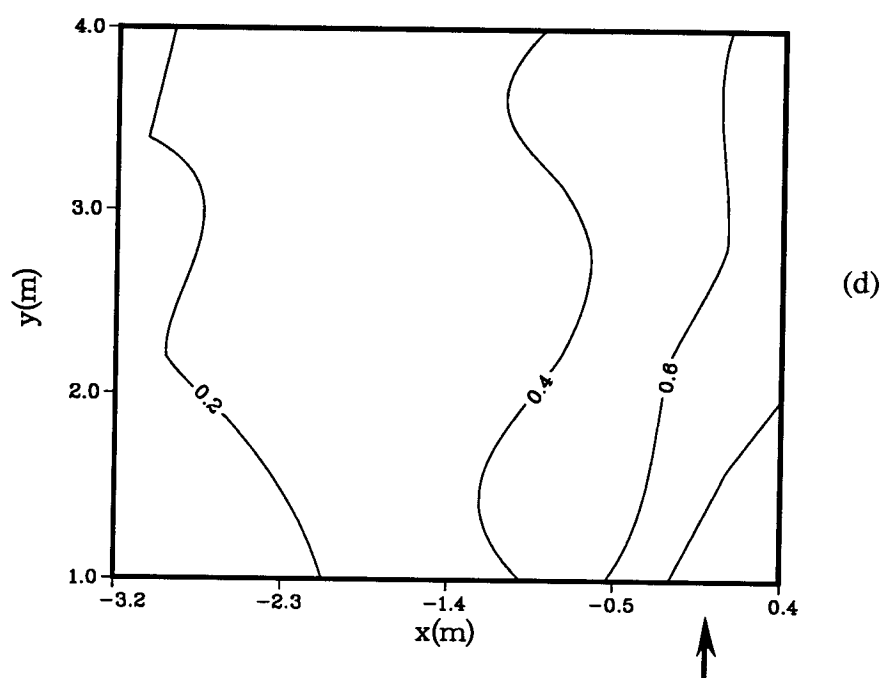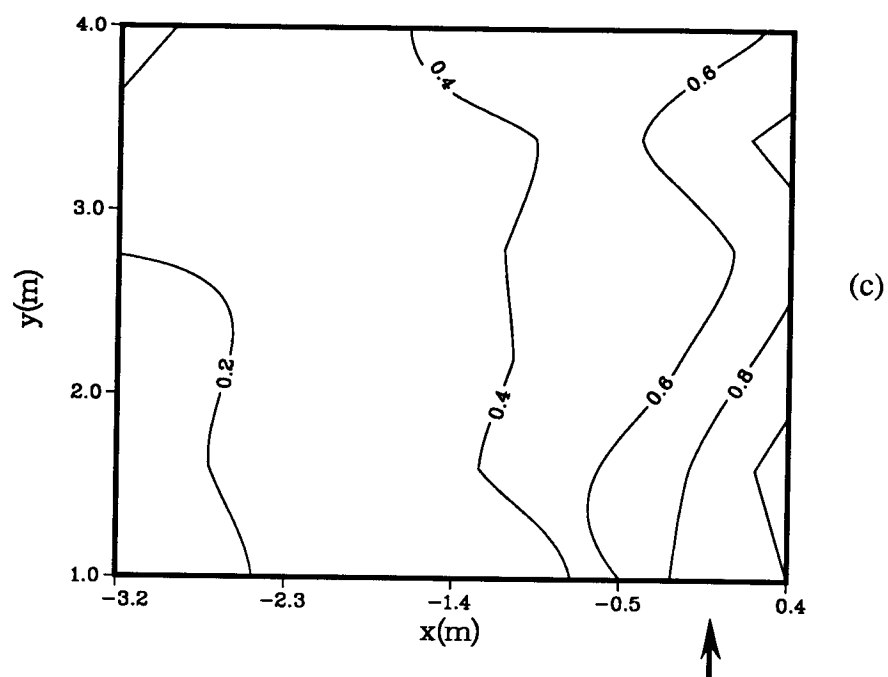
Figure 4.18   Continued.
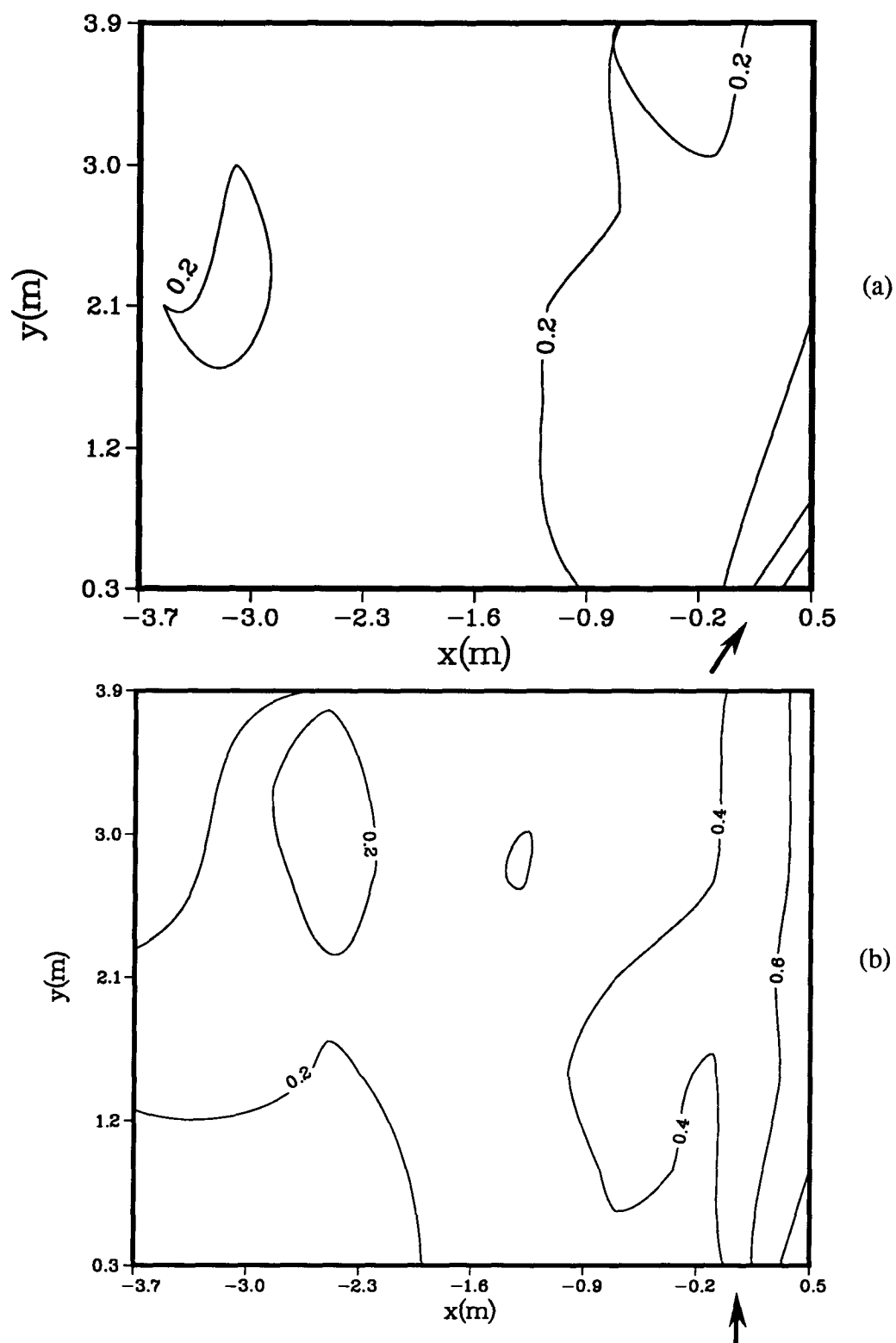
Figure 4.19   Diffraction coefficient contours for Phase 2 tests with T = 0.8 sec showing the effect of incident wave direction. (a) θ = -30°, (b) θ = 0°, (c) θ = +30°.
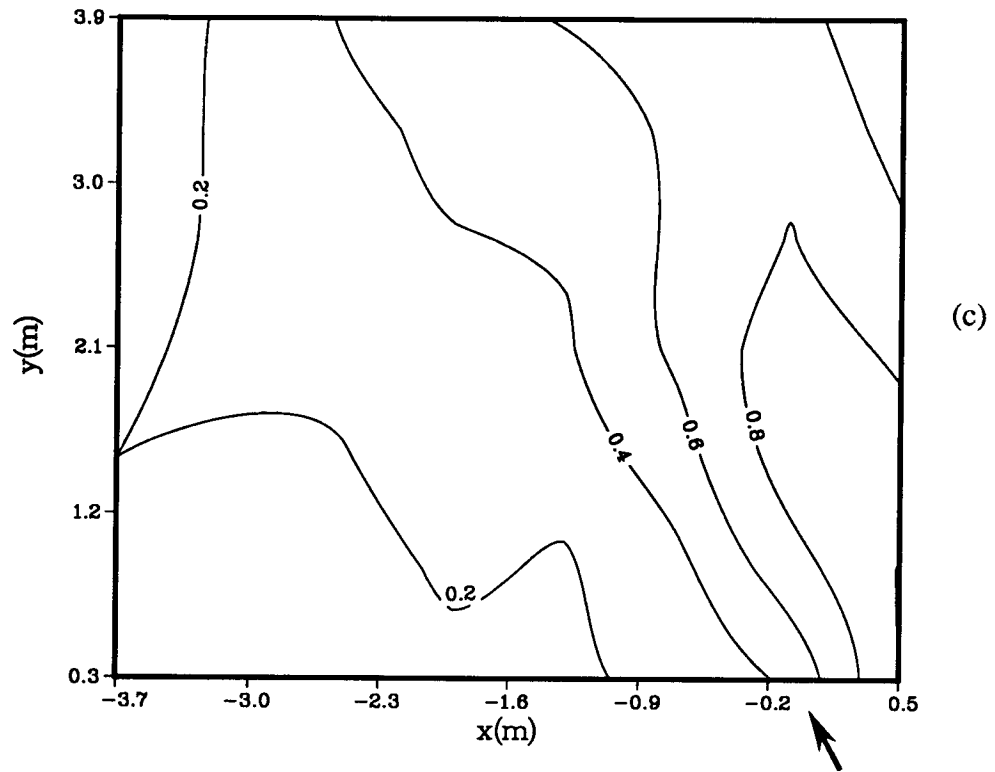
Figure 4.19   Continued.
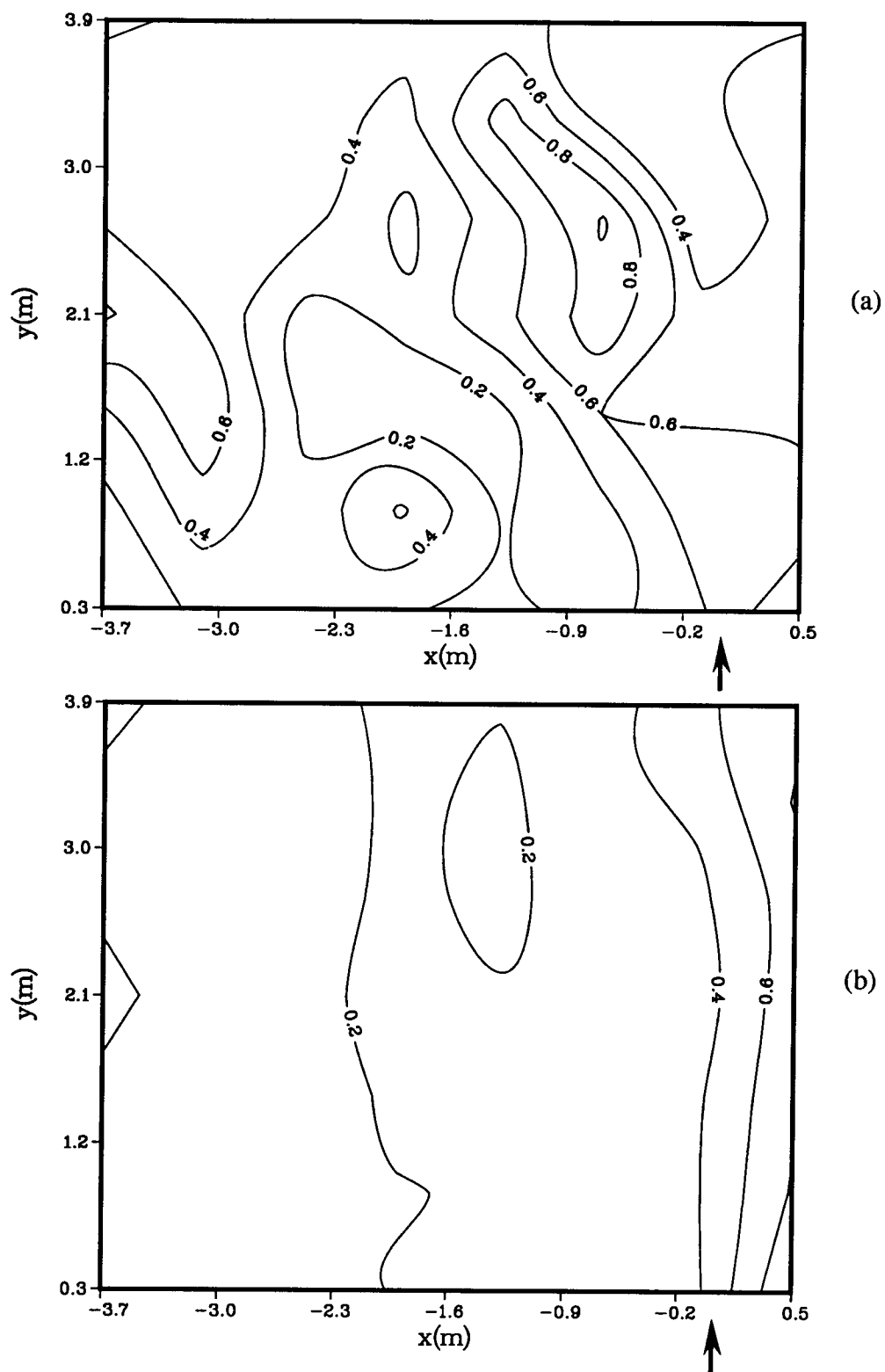
Figure 4.20   Diffraction coefficient contours for T = 0.94 sec, θ = 0° showing the effect of boundary reflection characteristics. (a) Phase 1, (b) Phase 2, (c) Phase 3.
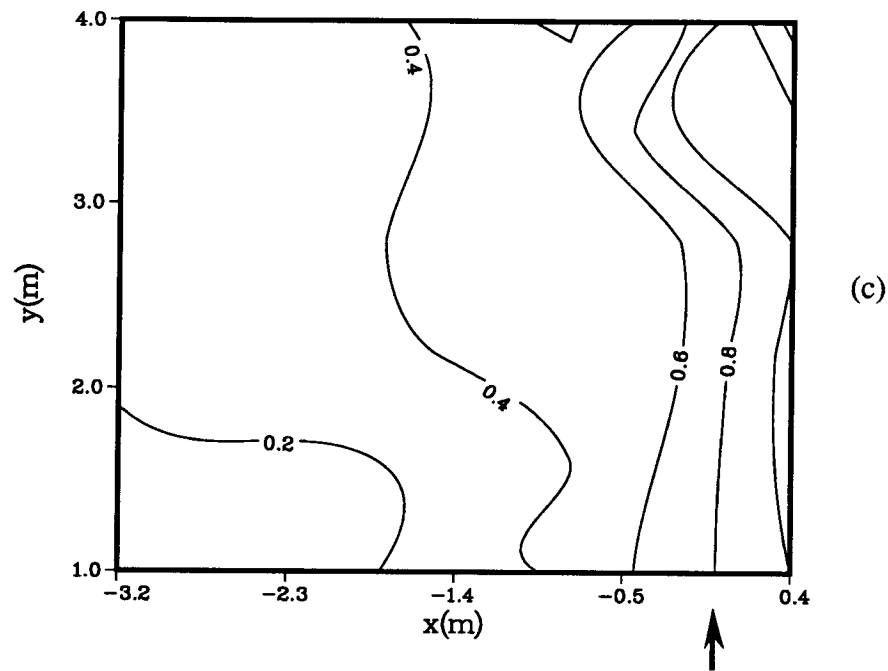
Figure 4.20   Continued.
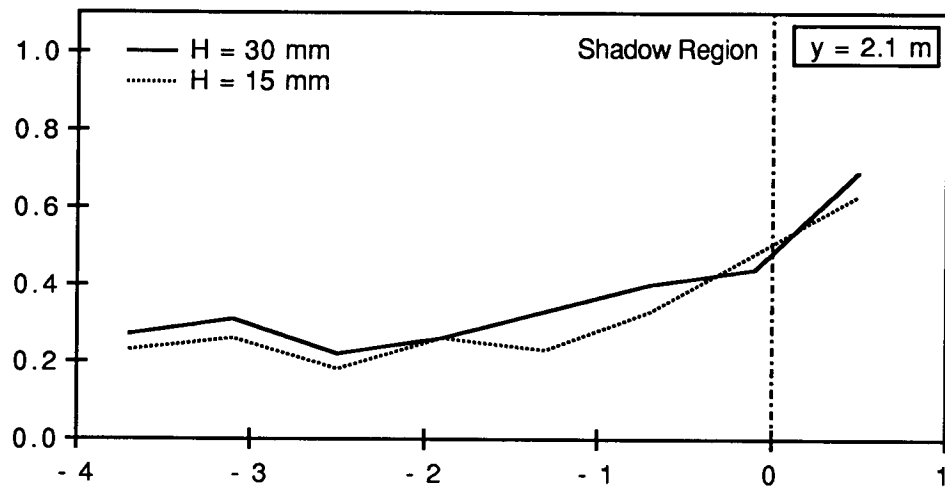
Figure 4.21   Diffraction coefficients along a traverse at y = 2.1 m
for Phase 2 tests with T = 0.8 sec and θ = 0°.
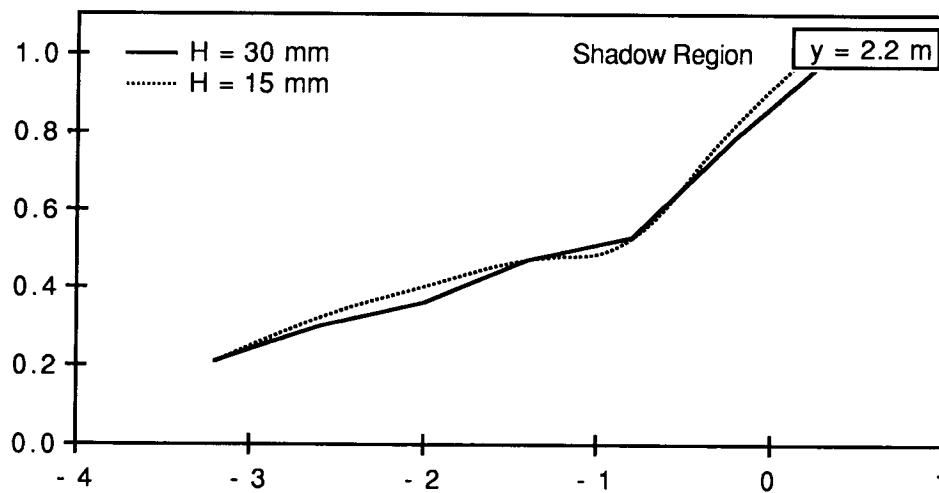
Figure 4.22   Diffraction coefficients along a traverse at y = 2.2 m
for Phase 3 with T = 0.8 sec and θ = 0°.
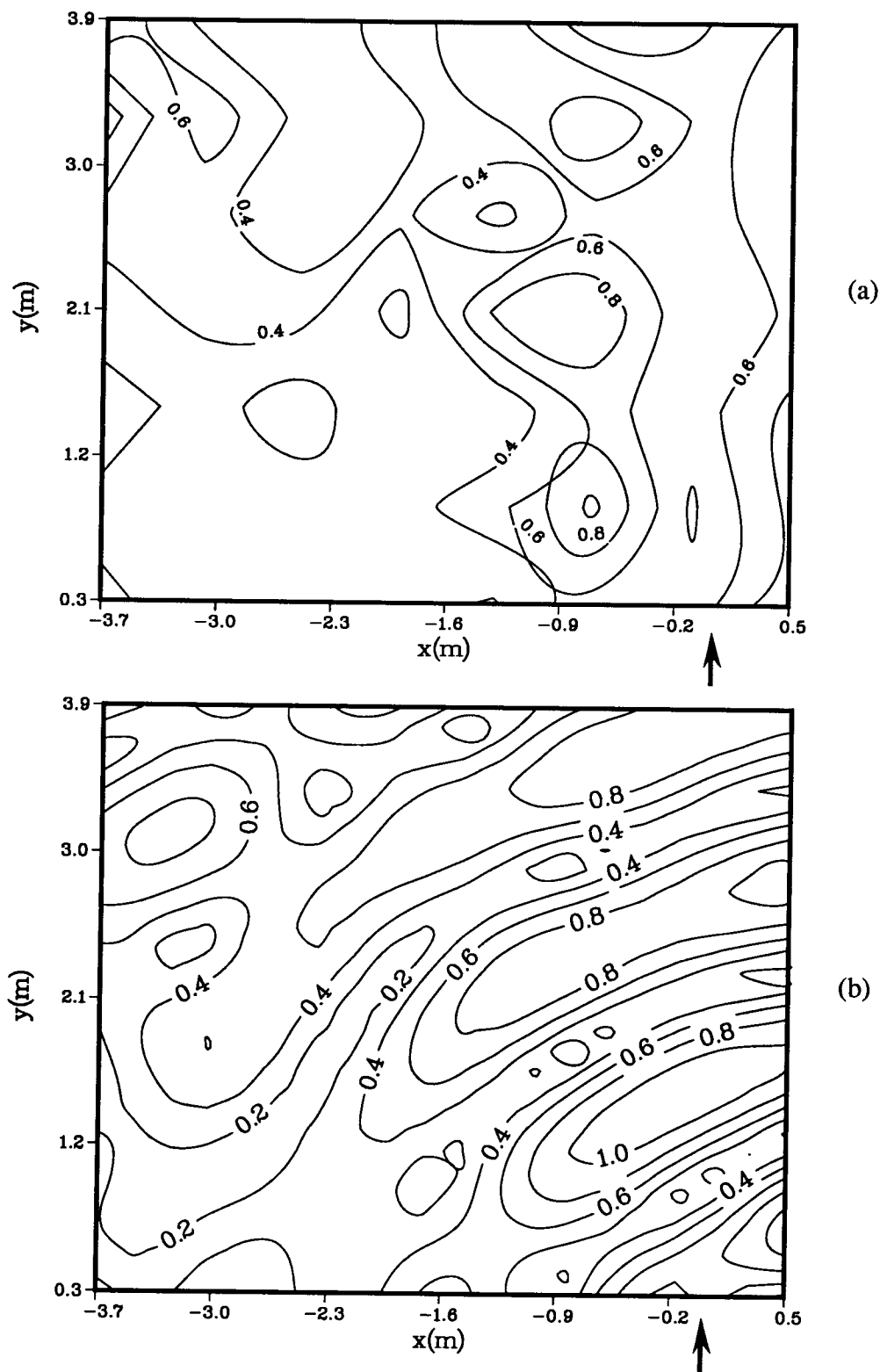
Figure 4.23   Diffraction coefficient contours for Phase 1 tests with T = 1.2 sec, θ = 0°.
   (a) experimental results, (b) numerical results.
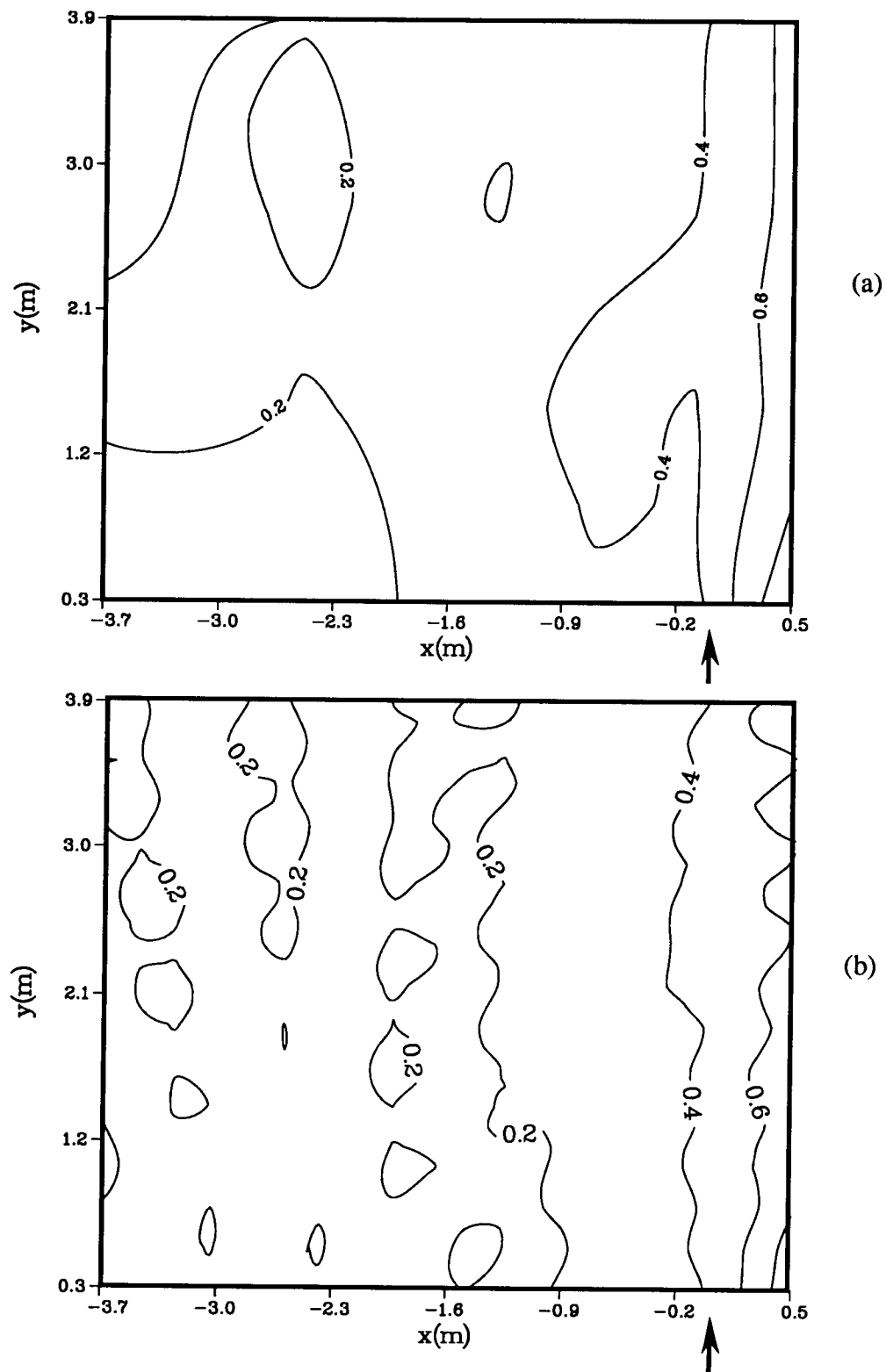
Figure 4.24   Diffraction coefficient contours for Phase 2 tests with T = 0.8 sec, θ = 0°.
(a) experimental results, (b) numerical results.
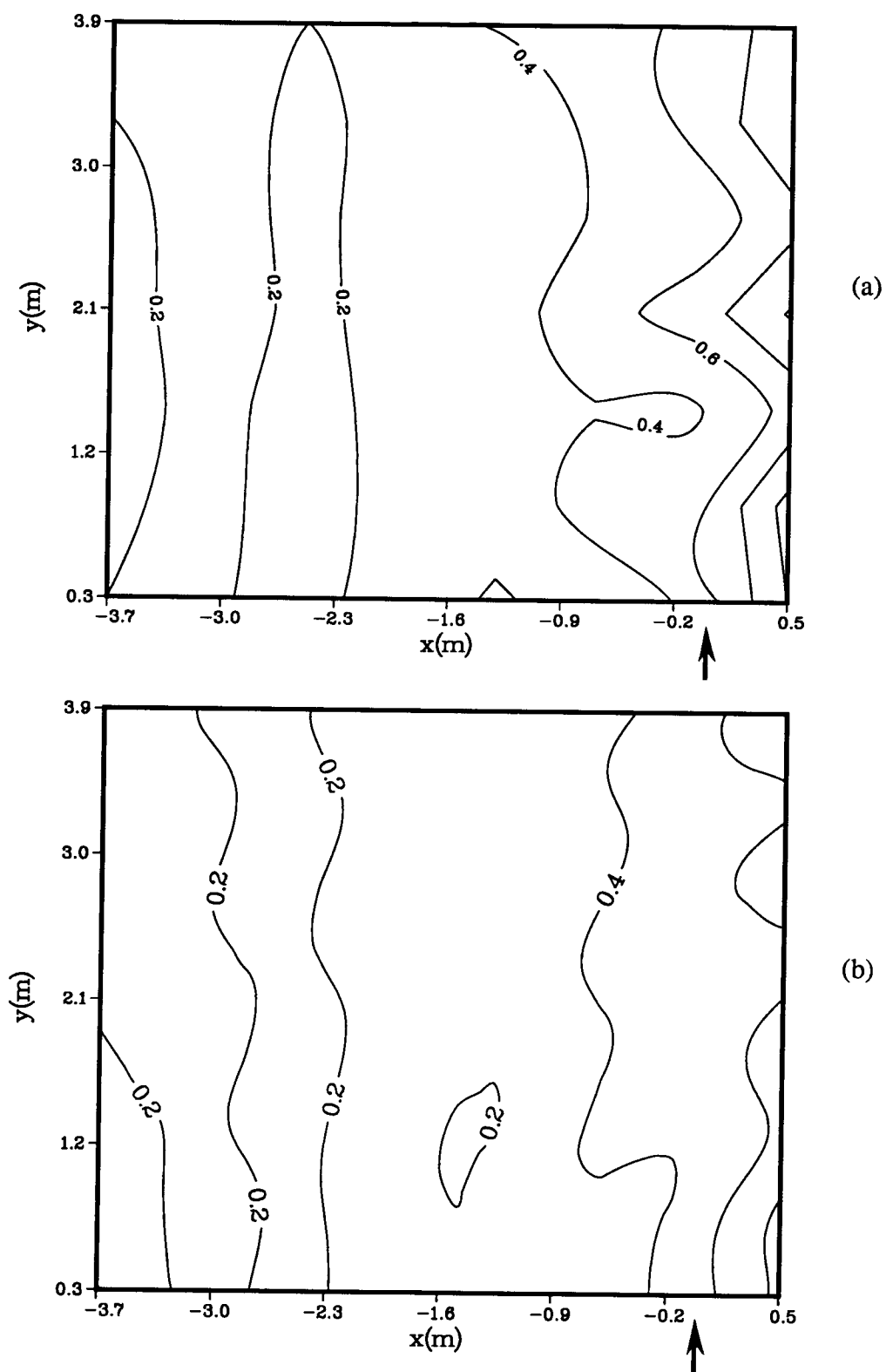
Figure 4.25   Diffraction coefficient contours for Phase 2 tests with T = 1.2 sec, θ = 0°.
(a) experimental results, (b) numerical results.
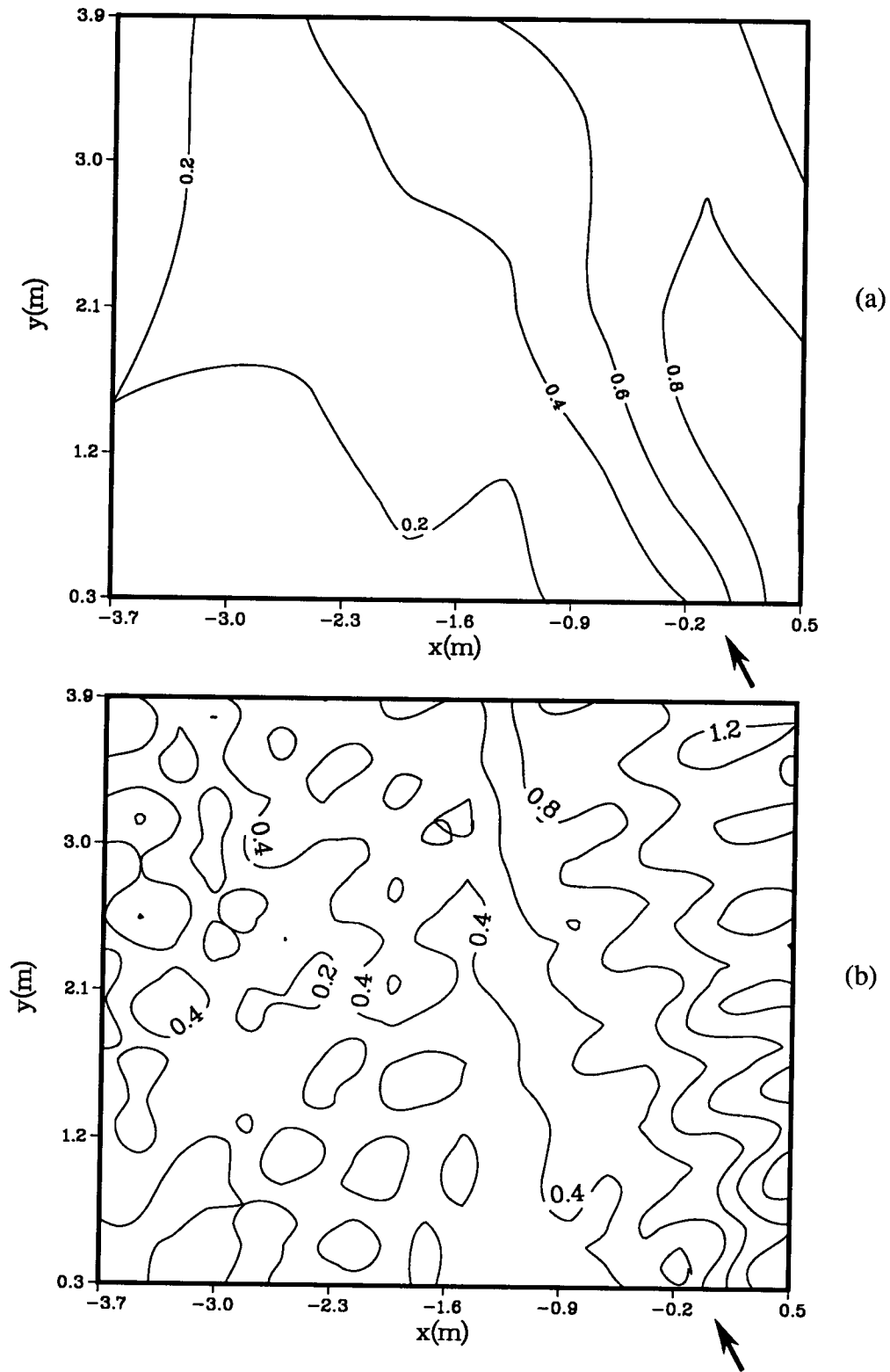
Figure 4.26   Diffraction coefficient contours for Phase 2 testswith T = 0.8 sec, θ = +30°.
(a) experimental results, (b) numerical results.

Photographs

Photograph 3.1   Experimental layout in the wave basin at BC Research.
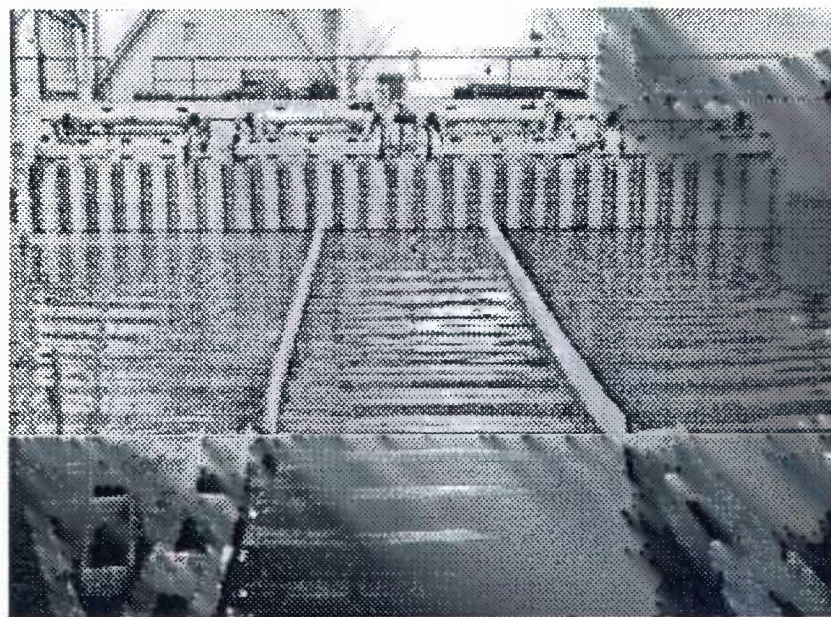
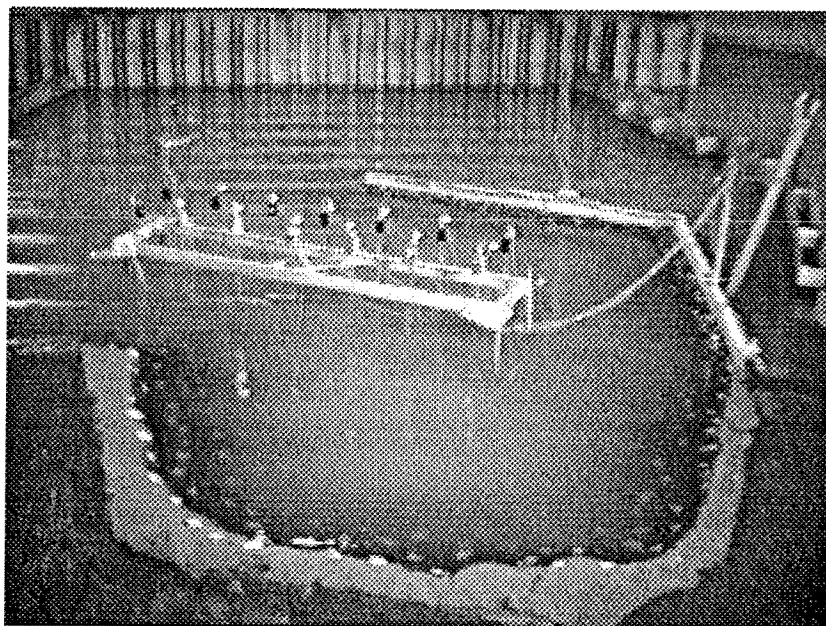Photograph 3.2   Wavemaker calibration in the wave basin at BC Research.

Photograph 3.3   Wavemaker calibration in the wave basin at BC Research.
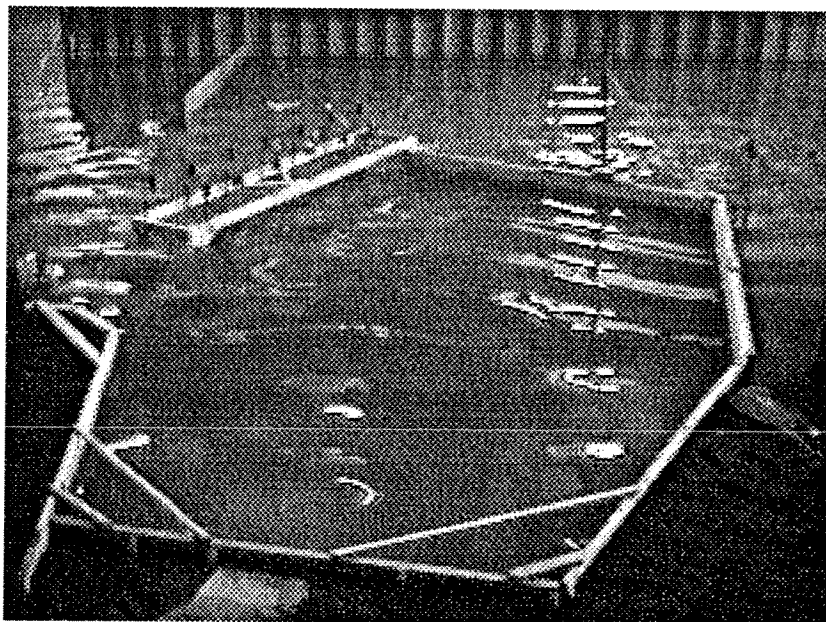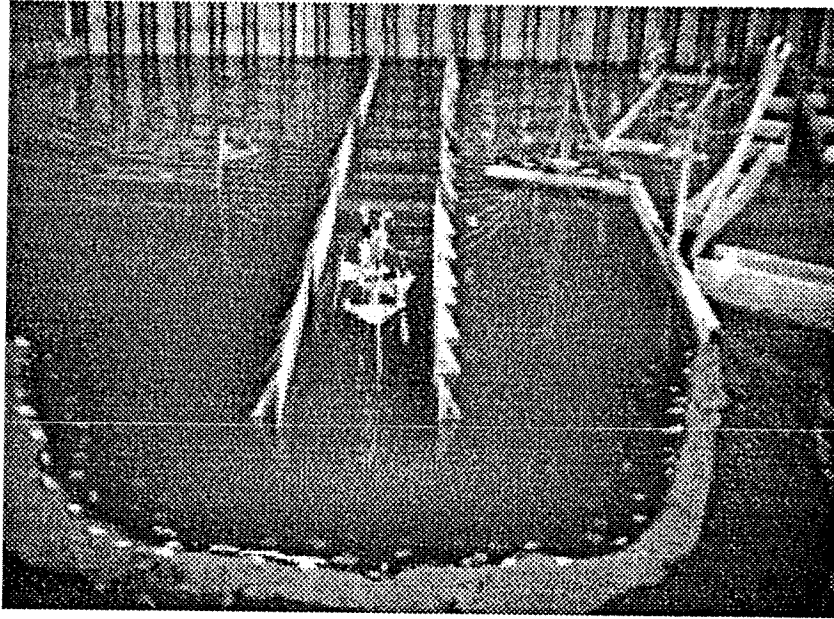

Photograph 3.4   Experimental layout for Phase 1 tests.
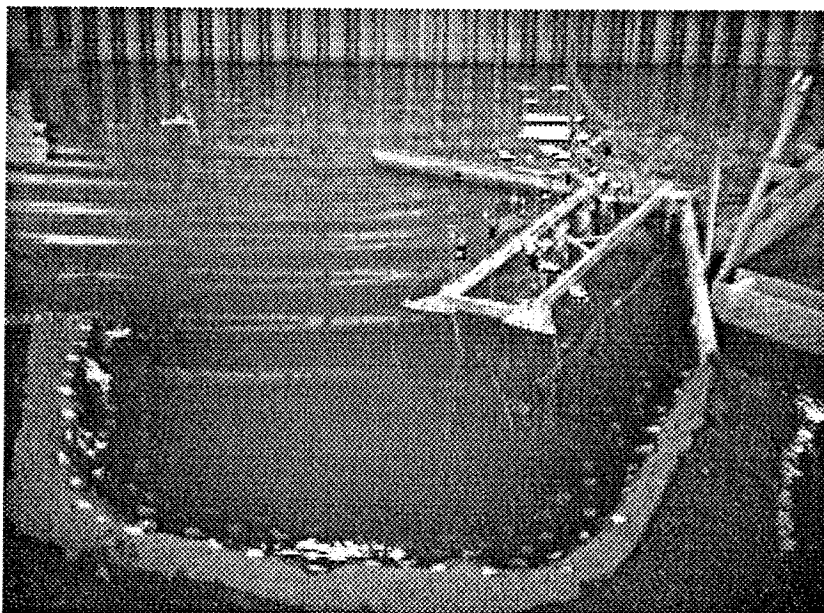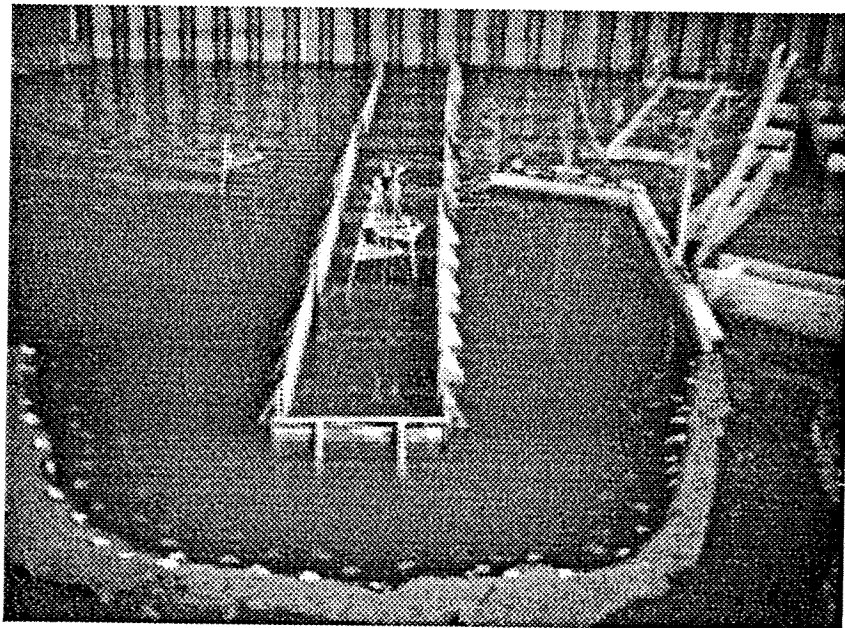
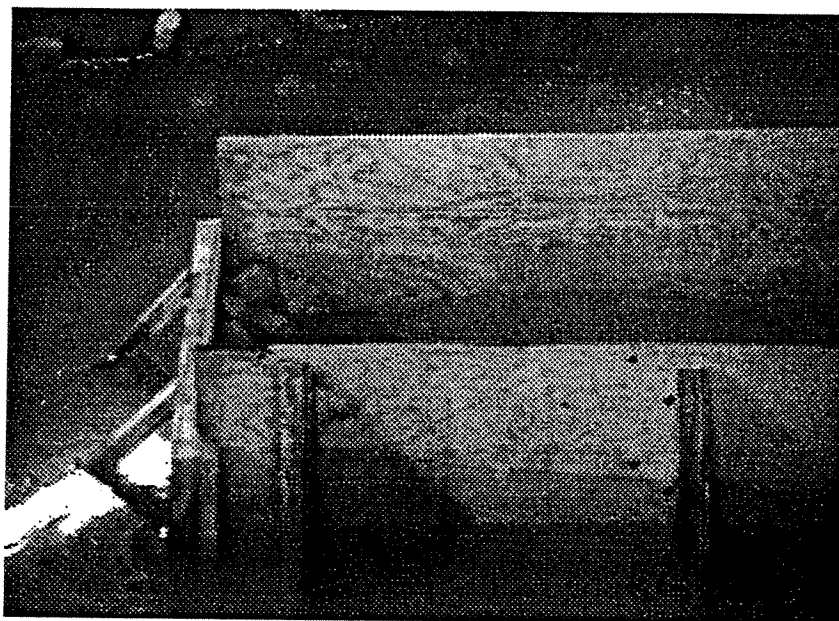Photograph 3.5   Experimental layout for Phase 2 tests.

Photograph 3.6   Experimental layout for Phase 3 tests.

Photograph 3.7   Measurement of the reflection coefficient of the sloping sand.

Photograph 3.8   Measurement of the reflection coefficient of the vertical plywood.

Photograph 3.9　　　Close-up of the measurement of the reflection coefficient of the rocks.